GOP-1 promotes apoptotic cell degradation by activating the small GTPase Rab2 in *C. elegans*

Jianhua Yin,[1,2,3]* Yaling Huang,[1]* Pengfei Guo,[1] Siqi Hu,[3] Sawako Yoshina,[5] Nan Xuan,[4] Qiwen Gan,[4] Shohei Mitani,[5] Chonglin Yang,[4] and Xiaochen Wang[1,2,3,6]

[1]National Institute of Biological Sciences, Beijing 102206, China
[2]Graduate Program in Chinese Academy of Medical Sciences and Peking Union Medical College, Beijing 100730, China
[3]National Laboratory of Biomacromolecules, CAS Center for Excellence in Biomacromolecules, Institute of Biophysics and [4]State Key Laboratory of Molecular Developmental Biology, Institute of Genetics and Developmental Biology, Chinese Academy of Sciences, Beijing 100101, China
[5]Deparment of Physiology, School of Medicine and Institute for Integrated Medical Sciences, Tokyo Women's Medical University, Tokyo 162-8666, Japan
[6]College of Life Sciences, University of Chinese Academy of Sciences, Beijing 100049, China

Apoptotic cells generated by programmed cell death are engulfed by phagocytes and enclosed within plasma membrane–derived phagosomes. Maturation of phagosomes involves a series of membrane-remodeling events that are governed by the sequential actions of Rab GTPases and lead to formation of phagolysosomes, where cell corpses are degraded. Here we identified *gop-1* as a novel regulator of apoptotic cell clearance in *Caenorhabditis elegans*. Loss of *gop-1* affects phagosome maturation through the RAB-5–positive stage, causing defects in phagosome acidification and phagolysosome formation, phenotypes identical to and unaffected by loss of *unc-108*, the *C. elegans Rab2*. GOP-1 transiently associates with cell corpse–containing phagosomes, and loss of its function abrogates phagosomal association of UNC-108. GOP-1 interacts with GDP-bound and nucleotide-free UNC-108/Rab2, disrupts GDI-UNC-108 complexes, and promotes activation and membrane recruitment of UNC-108/Rab2 in vitro. Loss of *gop-1* also abolishes association of UNC-108 with endosomes, causing defects in endosome and dense core vesicle maturation. Thus, GOP-1 is an activator of UNC-108/Rab2 in multiple processes.

Introduction

Phagocytic removal of apoptotic cells is important for tissue remodeling, suppression of inflammation, and regulation of immune responses (Savill and Fadok, 2000; Savill et al., 2002). In *Caenorhabditis elegans* hermaphrodites, 131 somatic cells and ∼50% of germ cells die through apoptosis, and the resulting cell corpses are phagocytosed and cleared by neighboring cells in the soma or by gonadal sheath cells that encase the germ line. During this process, apoptotic cells expose the phosphatidylserine "eat me" signal on the surface and are recognized and engulfed by phagocytes through evolutionarily conserved pathways, leading to cytoskeleton reorganization and formation of membrane-bound vesicles, namely phagosomes (Pinto and Hengartner, 2012; Wang and Yang, 2016). Maturation of cell corpse–enclosing phagosomes, which in many ways parallels endosome progression and maturation of phagosomes containing foreign bodies, involves sequential interactions with early endosomes, late endosomes, and lysosomes to yield phagolysosomes, where apoptotic cells are degraded (Flannagan et al., 2012; Wang and Yang, 2016).

As the key regulators of membrane trafficking, Rab GTPases act at multiple steps to mediate various membrane-remodeling events, leading to maturation of phagosomes and formation of phagolysosomes capable of digesting phagosomal contents (Flannagan et al., 2012; Gutierrez, 2013). In worms, four Rabs (RAB-5, UNC-108/Rab2, RAB-14, and RAB-7) function in a stepwise manner to promote phagosome maturation and cell corpse degradation. RAB-5 transiently associates with early phagosomes to promote phosphatidylinositol 3-phosphate (PtdIns3P) generation, probably by activating the phosphoinositide-3 kinase VPS-34, whereas RAB-7 is recruited later to mediate phagolysosome formation, probably through HOPS complex components (Kinchen et al., 2008; Yu et al., 2008; Xiao et al., 2009). Progression of phagosome maturation requires transition from RAB-5–positive early phagosomes to RAB-7–positive late phagosomes. The GTPase-activating protein TBC-2 inactivates RAB-5 to release it from phagosomal membranes, thereby promoting progression of phagosome maturation through the RAB-5–positive stage (Li et al., 2009). In addition, SAND-1/Monl acts with CCZ-1/Ccz1 to

*J. Yin and Y. Huang contributed equally to this work.

Correspondence to Xiaochen Wang: wangxiaochen@ibp.ac.cn

Abbreviations used: ANOVA, analysis of variance; DCV, dense core vesicle; DIC, differential interference contrast; GDI, GDP dissociation inhibitor; GEF, guanine nucleotide exchange factor; LG, linkage group; PtdIns3P, phosphatidylinositol 3-phosphate.

The Rockefeller University Press $30.00
J. Cell Biol. Vol. 216 No. 6 1775–1794
https://doi.org/10.1083/jcb.201610001

regulate RAB-5–to–RAB-7 transition, and thus promotes progression from the RAB-5–positive to the RAB-7–positive stage (Kinchen and Ravichandran, 2010). It is unclear whether TBC-2– and SAND-1/CCZ-1–dependent mechanisms coordinate and whether additional mechanisms are involved in this process.

UNC-108/Rab2 and RAB-14/Rab14 act in parallel to promote cell corpse degradation through phagosome maturation, but the exact steps at which they function remains unclear (Lu et al., 2008; Mangahas et al., 2008; Guo et al., 2010). UNC-108/Rab2 transiently associates with apoptotic cell–containing phagosomes, which requires RAB-5 function, suggesting that it acts downstream of RAB-5 activation (Guo et al., 2010). As well as removing apoptotic cells, UNC-108/Rab2 regulates endosome-to-lysosome maturation and maturation of dense core vesicles (DCVs; Chun et al., 2008; Lu et al., 2008; Edwards et al., 2009; Sumakovic et al., 2009). How UNC-108/Rab2 is recruited to and activated on the target membrane in phagosome, endosome, and DCV maturation processes remains unaddressed.

As the molecular switches for a variety of membrane trafficking events, Rab GTPases oscillate between GDP-bound inactive and GTP-bound active forms under the control of multiple regulatory proteins. Prenylated GDP-bound Rabs in the cytosol or on membranes are bound to GDP dissociation inhibitor (GDI), which delivers Rabs to and retrieves them from the target membrane (Seabra and Wasmeier, 2004). The membrane targeting and subsequent activation of Rab proteins require dissociation of Rabs from the GDI complex, followed by exchange of GDP for GTP catalyzed by guanine nucleotide exchange factor (GEF; Pfeffer and Aivazian, 2004; Seabra and Wasmeier, 2004; Barr, 2013). GTP-bound active Rabs interact with effector proteins to achieve downstream functions and are subsequently inactivated by GTPase activating protein (GAP), which promotes GTP hydrolysis and therefore cycles Rabs to the GDP-bound inactive state (Barr and Lambright, 2010). GDI extracts GDP-bound Rabs from the target membrane to stabilize them in the cytosol or return Rabs to the original membrane for further rounds of membrane insertion and Rab activation. GDP-bound prenylated Rabs associate tightly with GDI, and disruption of certain Rab–GDI complexes may be facilitated by GDI displacement factor (GDF; Pfeffer and Aivazian, 2004). Yip3/PRA1 has GDF activity toward endosomal Rabs, and loss of its function affects membrane association of Rab9 (Dirac-Svejstrup et al., 1997; Sivars et al., 2003). On the other hand, SidM/DrrA, a *Legionella* type IV effector, regulates membrane cycling of Rab1 by performing both GDI displacement and nucleotide exchange functions, indicating that GDF and GEF activity can be promoted by a single protein (Ingmundson et al., 2007; Machner and Isberg, 2007; Schoebel et al., 2009; Suh et al., 2010; Zhu et al., 2010). Whether eukaryotic proteins can catalyze coupled GDI displacement and nucleotide exchange like SidM/DrrA remains to be determined.

Here we identified GOP-1, a conserved protein homologous to *Drosophila melanogaster* Ema and human CLEC16A, as the activator of UNC-108/Rab2 to promote apoptotic cell clearance and maturation of endosomes and DCVs. Loss of GOP-1 abrogates recruitment of UNC-108/Rab2 to phagosomes and endosomes, causing defects in maturation of phagosomes, endosomes, and DCVs. GOP-1 interacts specifically with GDP-bound and nucleotide-free UNC-108/Rab2, disrupts GDI-UNC-108 complexes, and promotes activation and membrane association of UNC-108/Rab2 in vitro. Expression of human CLEC16A substitutes for GOP-1 function in all three processes, indicating conserved roles of this protein family in Rab2 activation.

Results

Loss of GOP-1 affects cell corpse clearance

UNC-108/Rab2 and RAB-14 function in parallel to promote cell corpse degradation (Guo et al., 2010). We performed a genome-wide RNAi screen to search for genes whose loss of function enhances the persistent cell corpse phenotype of *rab-14(lf)* mutants and thus may act in the same pathway with UNC-108/Rab2 to remove apoptotic cells. This screen identified *gop-1*, which encodes a conserved protein homologous to human CLEC16A (C-type lectin domain family 16, member A) and *Drosophila* Ema (endosomal maturation defective; Fig. S1 A). All three proteins contain a conserved uncharacterized domain (FPL domain) at the N terminus, followed by a predicted short transmembrane span (Fig. S1 A). CLEC16A has a putative sugar-binding C-type lectin domain that is not conserved in GOP-1 or Ema (Fig. S1 A; Kim et al., 2010).

We examined the appearance of cell corpses, which are identified by their raised button-like morphology and surface-exposed phosphatidylserine, in wild-type and *gop-1* mutants (Fig. 1 A; Wang et al., 2007; Cheng et al., 2017). We found that three deletion mutants of *gop-1* (*tm5384*, *tm5694*, and *tm5654*) and a nonsense mutant (*yq79*) that changes Arg 49 to a premature stop codon all contained significantly more cell corpses than wild type at various embryonic stages and in adult germline (Fig. 1, B and C; and Fig. S1, B–D). Because all *gop-1* alleles showed similar cell corpse phenotypes, we performed all subsequent experiments in *tm5384*, a deletion mutation of *gop-1* that causes an early stop codon after Ile 134 (Fig. S1 B). We found that cell deaths occurring 200–380 min after the first embryonic cleavage were similar in wild type and *gop-1(tm5384)*, indicating that *gop-1* mutants do not have excessive cell deaths (Fig. 1 D). In contrast, cell corpses persisted significantly longer in *gop-1* mutants than in wild type, suggesting that cell corpse removal is defective in *gop-1* mutants (Fig. 1, E and F). Expression of a GFP fusion of GOP-1 controlled by the *gop-1* promoter or the *ced-1* promoter, which drives gene expression in engulfing cells but not dying cells, fully rescued the persistent cell corpse phenotype in *gop-1(tm5384)* mutants, suggesting that GOP-1 acts in engulfing cells to promote cell corpse removal (Fig. S2, A and B). Consistent with this, GFP expression driven by the *gop-1* promoter ($P_{gop\text{-}1}$GFP) was observed from embryonic stages throughout larval and adult stages in several engulfing cell types such as pharyngeal muscle cells, intestine cells, and gonadal sheath cells (Fig. S3, A–D′ and G–H′). GFP expression was also seen in coelomocytes and dorsal and ventral nerve cord, consistent with the function of GOP-1 in endosome and DCV maturation (see below; Fig. S3, E–F′, I, and I′). Expression of human *CLEC16A* driven by the *ced-1* promoter efficiently rescued the cell corpse phenotype of *gop-1(tm5384)*, indicating that CLEC16A can substitute for *C. elegans* GOP-1 in removing apoptotic cells (Fig. S2, A and B).

GOP-1 acts in the same pathway with UNC-108 to promote phagosome maturation

unc-108;rab-14 double mutants contain significantly higher numbers of cell corpses than either of the single mutants alone (Fig. 1, G and H; Guo et al., 2010), indicating that these genes function in parallel to promote apoptotic cell clearance. We found that *gop-1(tm5384)* contained similar numbers of embryonic and germ cell corpses as *unc-108(n3263)*, *rab-14(tm2095)*,

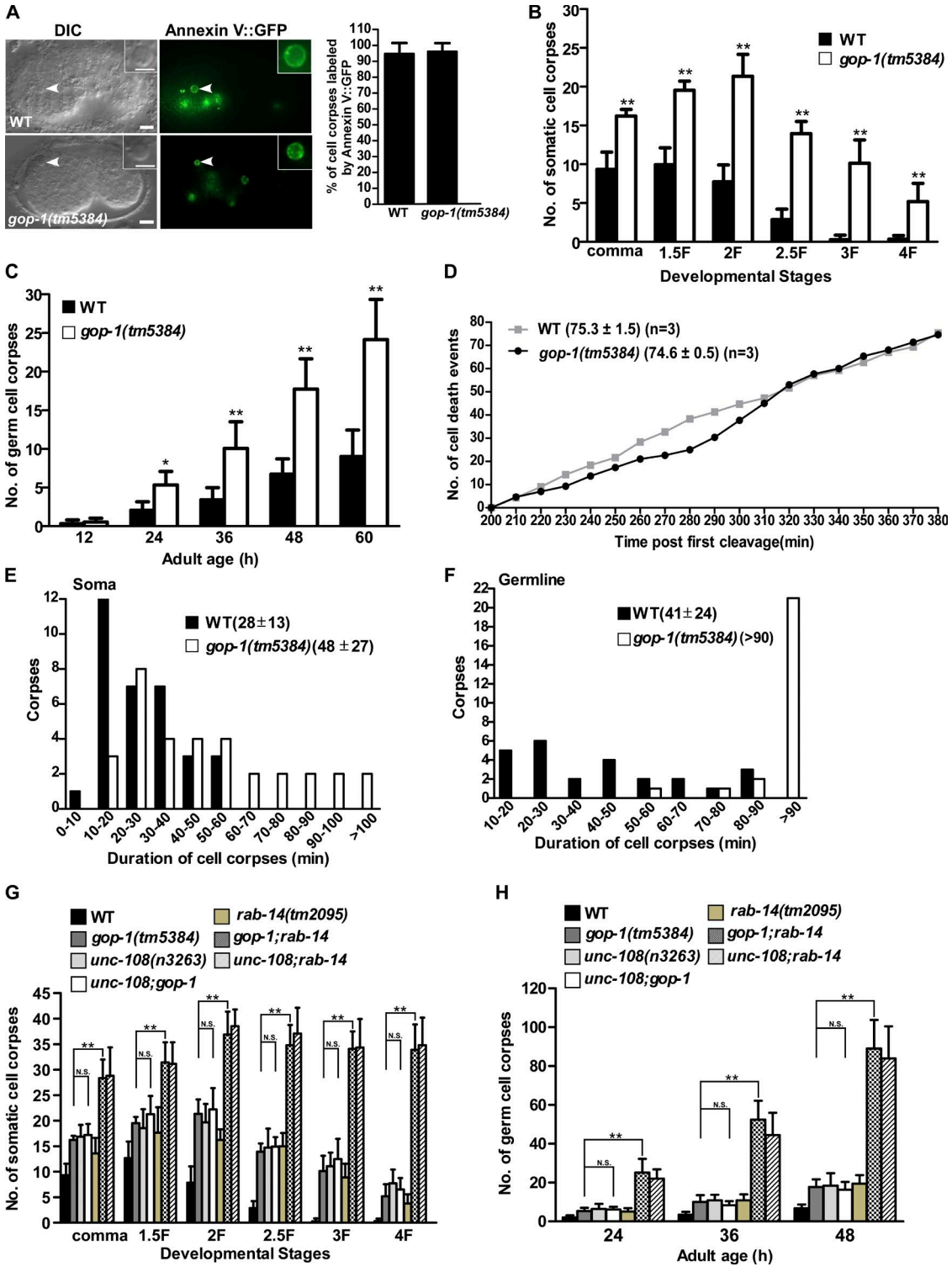

Figure 1. ***gop-1* is required for cell corpse removal.** (A) DIC and fluorescent images of wild-type and *gop-1(tm5384)* embryos expressing Annexin V::GFP. Cell corpses were identified by their raised button–like morphology and surface-exposed phosphatidylserine indicated by Annexin V::GFP labeling (arrowheads). The percentage of cell corpses labeled by Annexin V::GFP was quantified and is shown as mean ± SD at right. Unpaired *t* test was performed to compare data derived from wild type with that of *gop-1(tm5384)*. No significant difference was observed. Bar, 2.5 µm. (B, C, G, and H) Time-course analysis of cell corpse appearance during embryonic (B and G) and germline (C and H) development was performed in the indicated strains. The *y* axis indicates the number of cell corpses. At least 15 animals were scored in each strain at each stage, and data are shown as mean ± SD. Data derived from different genetic backgrounds at multiple developmental stages were compared by two-way ANOVA followed by Bonferroni posttest. *, $P < 0.05$; **, $P < 0.001$; N.S., not significant. (D) Embryonic cell deaths occurring 200–380 min after the first cleavage were followed in wild type (WT; $n = 3$) and *gop-1(tm5384)* mutants ($n = 3$). The mean number of total cell deaths (± SD) is shown in parentheses. The *y* axis indicates the number of cell deaths at each time point. (E and F) Cell corpse duration in soma (E) and germ line (F) was analyzed by 4D microscopy in WT and *gop-1(tm5384)* mutants. 33 somatic cell corpses or 25 germ cell corpses were examined in each strain. The mean duration time of cell corpses (± SD) is shown in parentheses.

or *unc-108;gop-1* worms, whereas *gop-1;rab-14* double mutants accumulated significantly more cell corpses than either of the single mutants alone or the *unc-108;gop-1* double mutants, a phenotype very similar to *unc-108;rab-14* (Fig. 1, G and H). These data suggest that GOP-1 functions in the same pathway with UNC-108 to remove cell corpses.

Cell corpses were similarly surrounded by the phagocytic receptor CED-1 or a plasma membrane reporter Myri-GFP in both wild type and *gop-1(tm5384)*, suggesting that recognition and initiation of engulfment are not affected (Fig. 2, A and B). However, more *gop-1(tm5384)* phagosomes were labeled by the early phagosome markers RAB-5 and 2xFYVE, the PtdIns3P biosensor, whereas association of the late phagosome marker RAB-7 and the lysosomal reporter LAAT-1 was greatly reduced, suggesting impaired phagosome maturation (Fig. 2, A, B, and P). Similar results were also observed in *unc-108(lf)* and *unc-108;gop-1* worms (Fig. 2, A, B, and P). The lumen of phagosomes enclosing apoptotic cells is gradually acidified during the maturation process, which requires parallel functions of UNC-108 and RAB-14 (Li et al., 2009; Guo et al., 2010). We found that significantly fewer germ cell corpses were labeled by Lysosensor green in *gop-1(tm5384)* worms, as in *unc-108(n3263)* or *rab-14(tm2095)* mutants, suggesting that *gop-1* is required for phagosomal acidification (Fig. 2, C–E′ and I). Loss of *gop-1* greatly enhanced the acidification defect in *rab-14(lf)* but not *unc-108(lf)* mutants (Fig. 2, F–I). The lysosomal membrane protein LAAT-1 was recruited to a majority of wild-type phagosomes, but the proportion of LAAT-1–positive phagosomes was significantly reduced in *gop-1(tm5384)*, *unc-108(n3263)*, or *rab-14(tm2095)* single mutants or *unc-108;gop-1* double mutants (Fig. 2, J–M′ and P). In *gop-1;rab-14* and *unc-108;rab-14* double mutants, recruitment of LAAT-1::GFP to phagosomes was almost completely blocked (Fig. 2, N–P). These data indicate that GOP-1 functions in the same pathway with UNC-108 and in parallel to RAB-14 to promote phagosomal acidification and phagolysosome formation.

Loss of GOP-1 and UNC-108 affects phagosome progression through the RAB-5–positive stage

To further examine the phagosome maturation process in *gop-1(lf)* and *unc-108(lf)*, we performed time-lapse analyses to follow the dynamics of RAB-5 and PtdIns3P on phagosomes. In wild type, RAB-5 and 2xFYVE appeared on phagosomes transiently, with a mean duration of 4.7 and 6.8 min, respectively (Videos 1 and 3 and Fig. 3, A–D). In *gop-1(tm5384)*, however, RAB-5 and 2xFYVE persisted significantly longer on phagosomes, with a mean duration of 15.2 and 65 min (Videos 2 and 4 and Fig. 3, A–D). The phagosomal duration of RAB-5 and 2xFYVE was also prolonged in *unc-108(n3263)* mutants (Fig. 3, A–D). These data suggest that loss of GOP-1 and UNC-108 may affect progression of phagosome maturation through the RAB-5–positive stage. To examine this, we followed the dynamics of RAB-7 and LAAT-1, which are recruited to phagosomes at late maturation steps. In wild type, RAB-7 associated with phagosomes for a mean of 51 min, and RAB-7–positive phagosomes shrank gradually in size and eventually disappeared, indicating completion of cell corpse degradation and recycling of phagosomal membranes (Fig. 4 A). In *unc-108(n3263)* and *gop-1(tm5384)* worms, however, most phagosomes were transiently associated with RAB-7, with a mean duration of 18.1 and 21.3 min (Fig. 4 A). Moreover, *unc-108* and *gop-1* phagosomes failed to shrink, consistent with defects in phagosome maturation and cell corpse degradation (Fig. 4 A). MTM-1 is a plasma membrane–localizing PtdIns3P phosphatase that associates with forming phagosomes and is released after they seal (Cheng et al., 2015). In wild type, LAAT-1 appeared on the phagosomal surface 5.4 min after phagosome sealing, as indicated by MTM-1 release, and the LAAT-1–positive phagosome gradually shrank (Fig. 4 B). In *unc-108(n3263)* and *gop-1(tm5384)* mutants, MTM-1 release was unaffected, but LAAT-1 recruitment was severely impaired (Fig. 4, C–F). LAAT-1 was absent from 53% and 41% of phagosomes in *unc-108(n3263)* and *gop-1(tm5384)*, respectively (Fig. 4, C and E), whereas 47% and 59% of *unc-108(n3263)* and *gop-1(tm5384)* phagosomes failed to recruit LAAT-1 until 26 and 23.9 min after MTM-1 release, which was significantly later than wild type (5.4 min; Fig. 4, B, D, and F). Together, these data suggest that loss of GOP-1 and UNC-108 affects progression of phagosome maturation through the RAB-5–positive stage, causing impaired RAB-7 association and phagolysosome formation.

TBC-2 is the GAP of RAB-5 that inactivates RAB-5 to promote phagosome maturation. Loss of *tbc-2* causes prolonged phagosomal accumulation of RAB-5 and PtdIns3P and impaired RAB-7 recruitment, phenotypes closely resembling those in *gop-1(lf)* and *unc-108(lf)* mutants (Li et al., 2009; Fig. 3, A–D). We found that loss of *tbc-2* significantly enhanced the cell corpse phenotype in *gop-1(lf)* and *unc-108(lf)* embryos and further extended the duration of RAB-5 and 2xFYVE on *unc-108(n3263)* phagosomes (Fig. 3, A–D; and Table S1). Loss of *tbc-2* in germ line, however, did not obviously affect clearance of germ cell corpses or alter the cell corpse numbers in *gop-1* and *unc-108* mutants, suggesting that TBC-2 plays a major role in removing embryonic but not germ cell corpses (Table S2). SAND-1/Mon1 regulates the switch from RAB-5–positive to RAB-7–positive phagosomes in the *C. elegans* germ line (Kinchen and Ravichandran, 2010). Loss of *sand-1* significantly increased germ cell corpse numbers in *gop-1(lf)* and *unc-108(lf)* worms (Table S2). These data suggest that GOP-1 and UNC-108 function in parallel to TBC-2 and SAND-1 to promote phagosome progression through the RAB-5–positive stage.

GOP-1 transiently associates with phagosomes, and loss of its function disrupts phagosomal recruitment of UNC-108

GFP::GOP-1 displayed both cytoplasmic and vesicular localization patterns, with the majority of GOP-1–positive puncta containing UNC-108, suggesting colocalization of the two proteins (Fig. 5, A–A″). The GOP-1– and UNC-108–positive vesicles either overlapped with or were near puncta labeled by FAPP1-PH, the trans-Golgi marker, suggesting that they localize to the trans-Golgi or vesicles closely associated with it (Fig. 5, B–C″). GOP-1 was absent from lysosomes (NUC-1), whereas a few GOP-1–positive vesicles colocalized with or were near RAB-5–positive early endosomes and RAB-7–positive late endosomes (Fig. S3, J–L″).

We observed GFP::GOP-1 rings surrounding apoptotic cells, suggesting that GOP-1 associates with phagosomes (Fig. 5, D, D′, G, and G′). *rab-5* RNAi but not *rab-7* RNAi or loss of *unc-108* disrupted phagosomal association of GOP-1, indicating that RAB-5 function but not RAB-7 or UNC-108 is required for recruiting GOP-1 to phagosomes (Fig. 5, E–K). Loss of *tbc-2*, which causes persistent activation of RAB-5 and

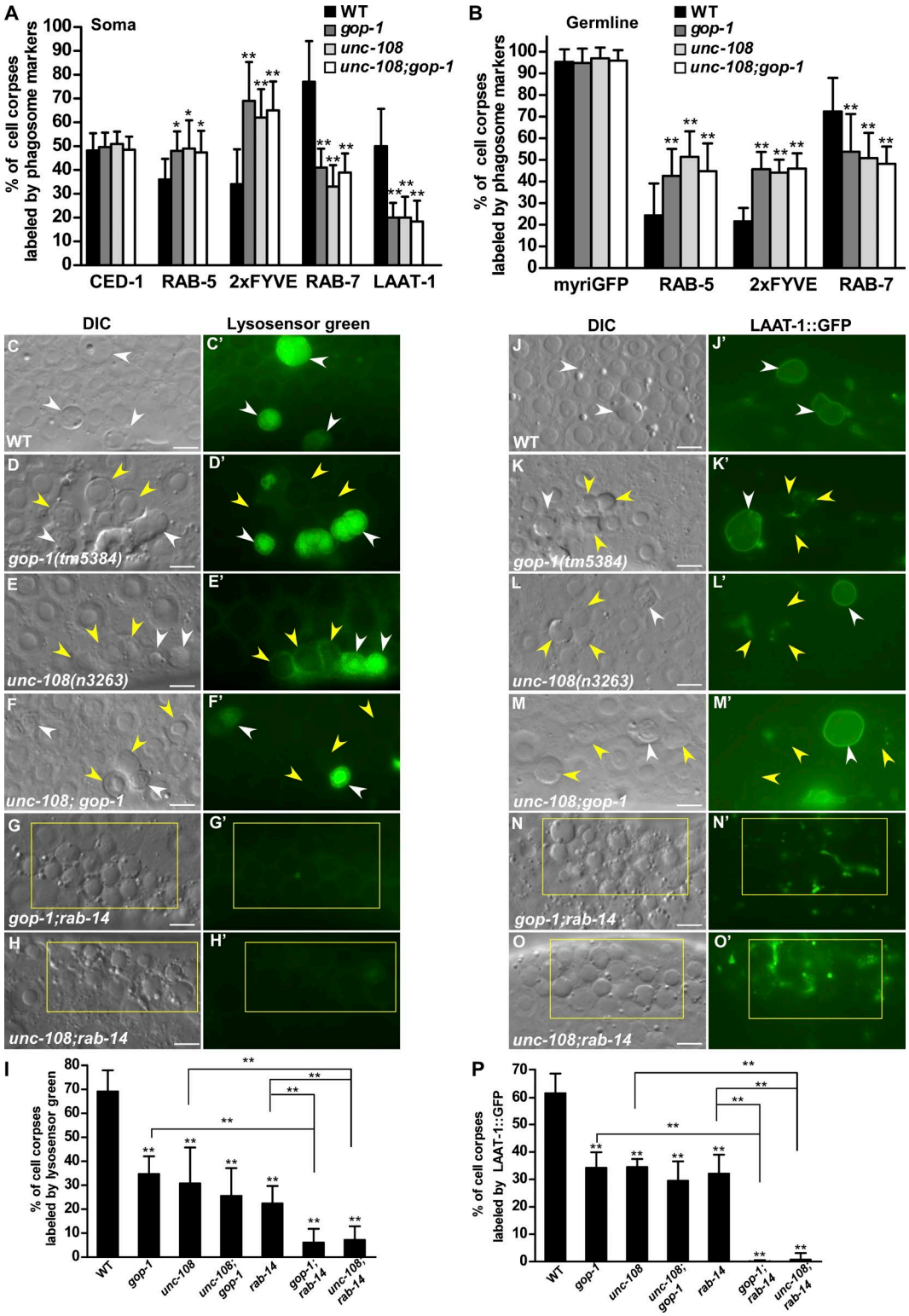

Figure 2. ***gop-1*and *unc-108* act in the same pathway to regulate phagosome maturation.** (A and B) Percentage of somatic (A) and germ cell corpses (B) labeled by various phagosomal markers at the 1.5-fold (A) or adult (48 h after L4/adult molt; B) stage was quantified in the indicated strains. (C–P) DIC and fluorescent images of the gonads stained by Lysosensor green (C–H′) or expressing LAAT-1::GFP (J–O′) in the indicated strains. White arrowheads, cell corpses labeled by Lysosensor green or LAAT-1::GFP; yellow arrowheads and boxes, unlabeled corpses. Quantification is shown in I and P. In A, B, I, and P, at least 15 animals were scored in each strain, and data are shown as mean ± SD. In A and B, data derived from different genetic backgrounds were compared by two-way ANOVA followed by Bonferroni posttest. *, $P < 0.05$; **, $P < 0.001$. All other points had $P > 0.05$. In I and P, one-way ANOVA with Tukey's posttest was performed to compare mutant datasets with wild type or datasets linked by lines. **, $P < 0.0001$. Bars, 5 µm.

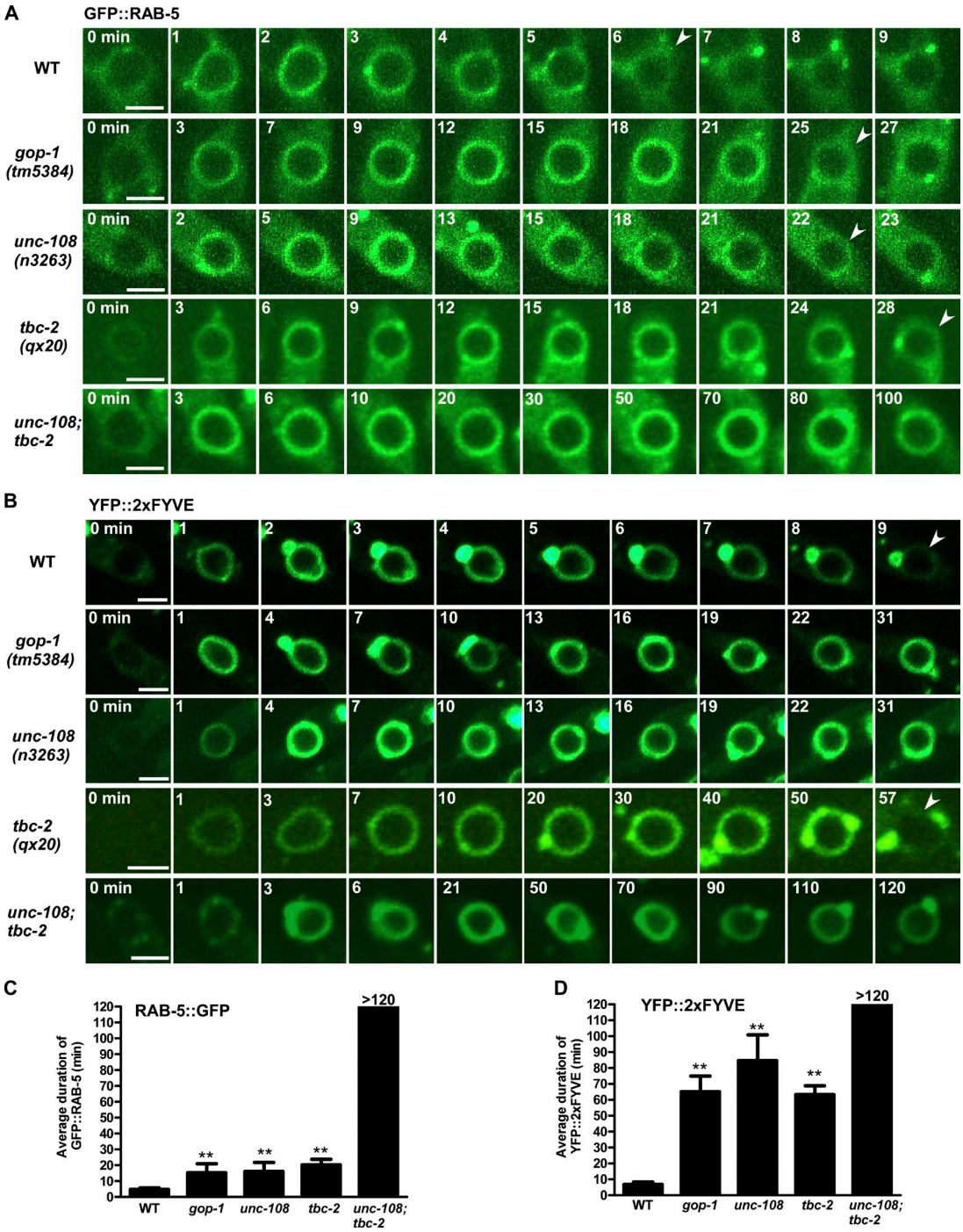

Figure 3. **Loss of *gop-1* and *unc-108* affects the dynamics of RAB-5 and PtdIns3P on phagosomes.** Time-lapse images of somatic cell corpses in wild type (WT), *gop-1(tm5384)*, *unc-108(n3263)*, *tbc-2(qx20)*, and *unc-108;tbc-2* embryos expressing GFP::RAB-5 (A) or YFP::2xFYVE (B). 0 min, time point before RAB-5 or FYVE was first detected around the cell corpse; arrowheads, time point when GFP::RAB-5 or YFP::2xFYVE disappears from phagosomes. Bars, 2.5 µm. Quantifications are shown in C and D. Data are shown as mean ± SD. One-way ANOVA with Tukey's posttest was performed to compare mutant datasets with wild type. **, P < 0.0001.

sustained PtdIns3P accumulation on phagosomes, led to an increase in GOP-1–positive phagosomes (Fig. 5, F, F′, J, and K).

We next investigated whether GOP-1 is responsible for recruiting UNC-108 to phagosomes. UNC-108 was recruited to phagosomes shortly after MTM-1 release and stayed on them for ∼6.2 min in wild-type embryos (Video 5 and Fig. 6, A and F). This indicates that UNC-108 is recruited to and transiently associates with fully sealed phagosomes, consistent with its role in phagosome maturation. In *gop-1(tm5384)* embryos, however, MTM-1 dynamics were unaffected, but UNC-108 was not recruited to phagosomes (Video 6 and Fig. 6, B and F). Similarly, UNC-108 was enriched transiently on phagosomes enclosing germ-cell corpses in wild-type sheath cells but was absent from phagosomes in *gop-1(tm5384)* worms (Fig. 6, C–E and G). These data indicate that GOP-1 is required to recruit UNC-108 to phagosomes.

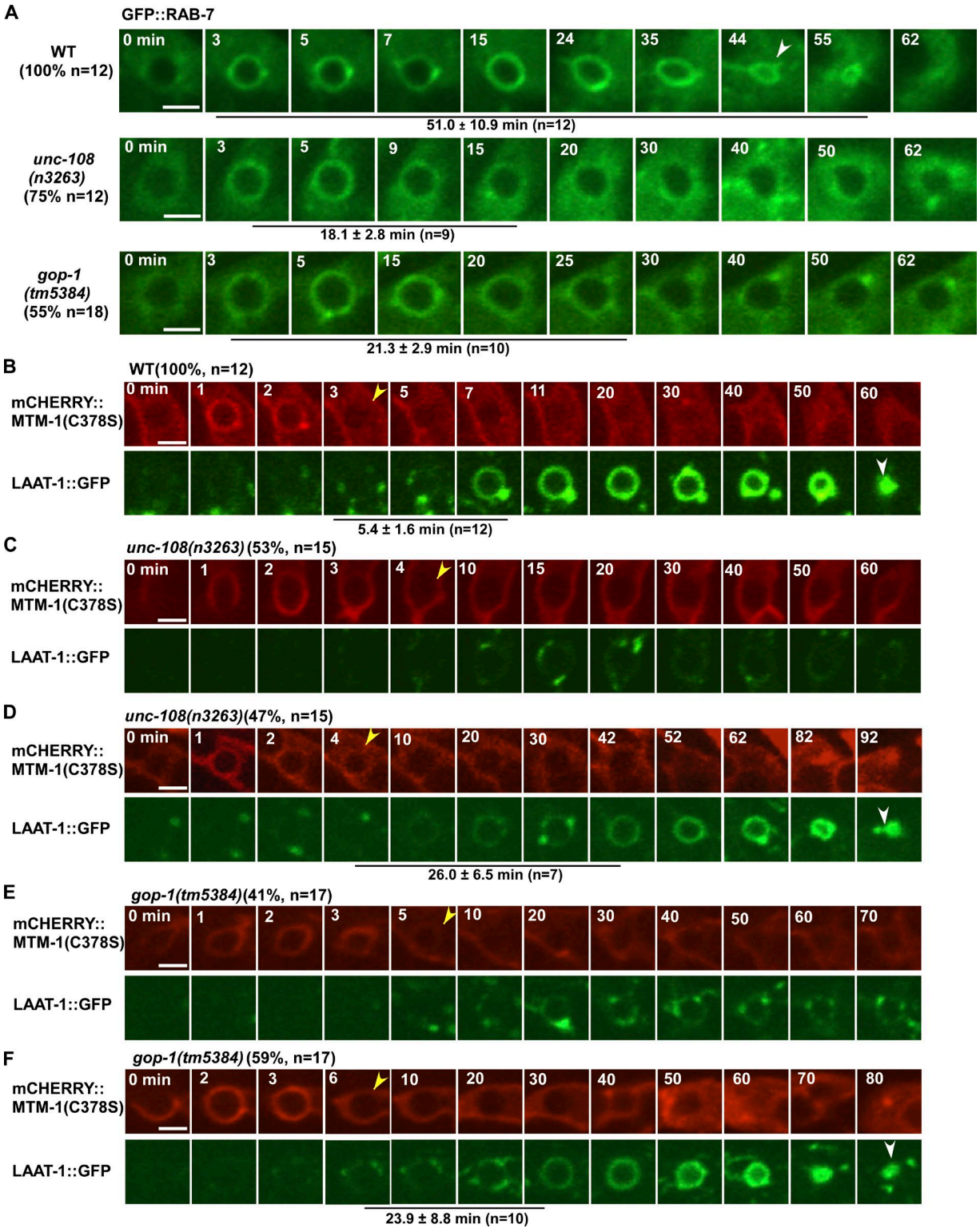

Figure 4. **Loss of *gop-1* and *unc-108* affects phagosomal association of RAB-7 and phagolysosome formation.** Time-lapse images of somatic cell corpses in wild type (WT), *unc-108(n3263)*, and *gop-1(tm5384)* embryos expressing GFP::RAB-7 (A) or coexpressing mCherry::MTM-1(C378S) and LAAT-1::GFP (B–F). 0 min, time point before RAB-7 or MTM-1 was first detected around the cell corpse; yellow arrowheads, MTM-1 release from phagosomes; white arrowheads, shrinkage of RAB-7– or LAAT-1–positive phagosomes. The percentage of phagosomes with the representative pattern is shown at left (A) or top (B–F). Quantification of RAB-7 duration on phagosomes (A) or the time between MTM-1 release and LAAT-1 recruitment is shown beneath the images (mean ± SD). *n*, number of phagosomes quantified. Bars, 2.5 µm.

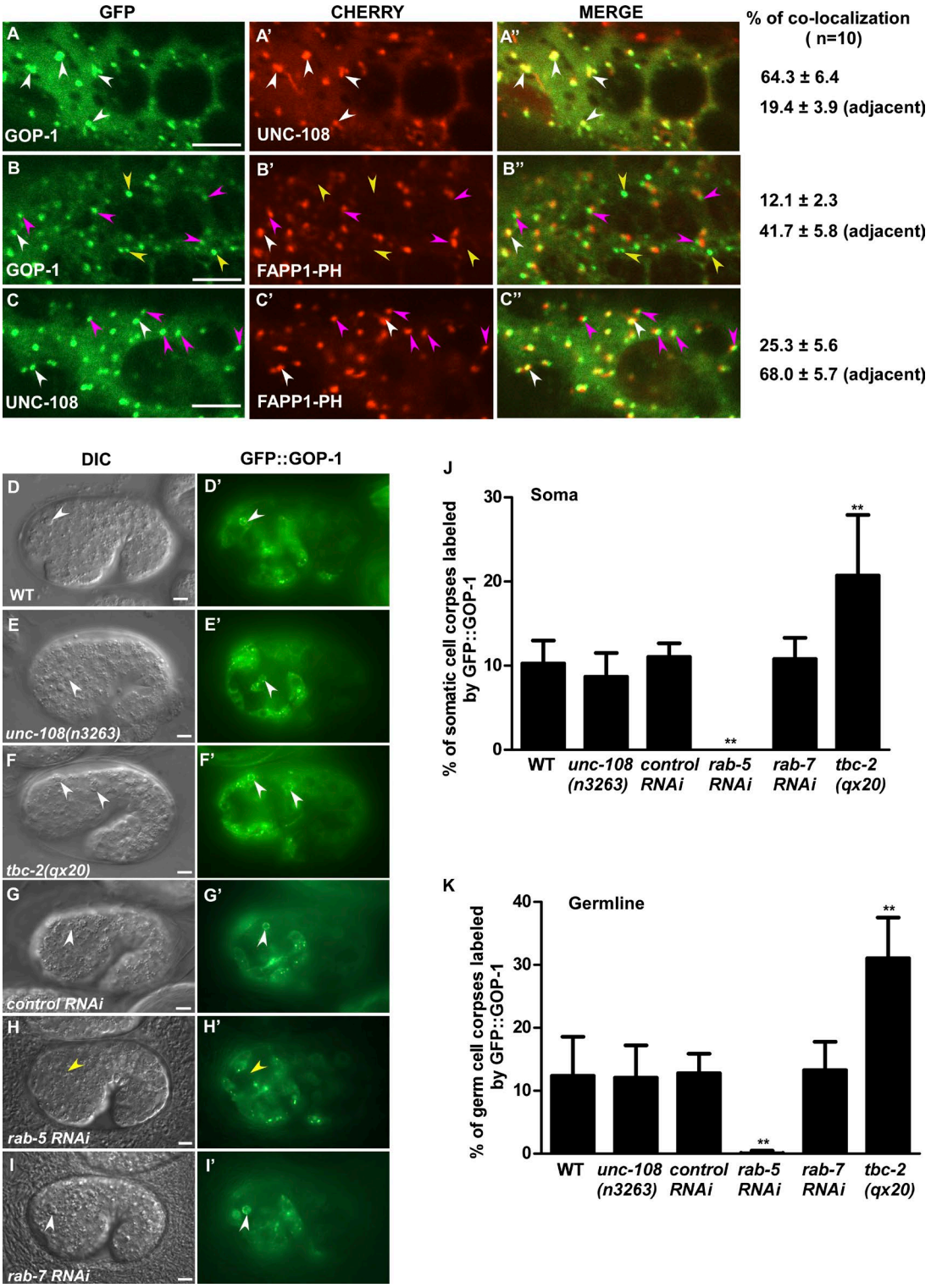

Figure 5. **Recruitment of GOP-1 to phagosomes requires RAB-5 but not RAB-7 function.** (A–C″) Confocal fluorescence images of the sheath cell in wild type coexpressing GFP::GOP-1 and Cherry::UNC-108 (A–A″) or Cherry::FAPP1-PH (B–B″, trans-Golgi marker) or coexpressing GFP::UNC-108 and Cherry::FAPP1-PH (C–C″). White arrowheads, vesicles containing overlapping GFP and Cherry fluorescence; pink arrowheads, GFP- and Cherry-positive vesicles that are in close proximity; yellow arrowheads, GFP-positive and Cherry-negative puncta. Quantification is shown at right. At least 10 animals were scored in each strain. Data are shown as mean ± SD. (D–I′) DIC and fluorescence images of embryos expressing GFP::GOP-1 in the indicated strains. White arrowheads, cell corpses labeled by GFP::GOP-1; yellow arrowheads, unlabeled ones. (J and K) Quantification of somatic (J) and germ cell (K) corpses labeled by GFP::GOP-1 in the indicated strains is shown. At least 15 animals were scored in each strain. Data are shown as mean ± SD. Recruitment of GOP-1 in *unc-108(n3263)* and *tbc-2(qx20)* was compared with that in wild type, whereas data derived from *rab-5* RNAi or *rab-7* RNAi were compared with the control group by unpaired *t* tests. **, $P < 0.0001$. All other points had $P > 0.05$. Bars, 5 µm.

GOP-1 acts together with UNC-108 to promote endosome and DCV maturation

In addition to removing apoptotic cells, UNC-108/Rab2 plays important roles in endosome and DCV maturation. Loss of UNC-108 affects endocytic trafficking, causing accumulation of aberrant endosome/lysosome hybrids (Chun et al., 2008; Lu et al., 2008). We found that *gop-1(tm5384)* worms contained enlarged vacuoles in coelomocytes, a phenotype that was efficiently rescued by expression of GOP-1::GFP (Fig. 7, A and B; and Fig. S2, C–E and H). Similar to *unc-108(lf)*, the large vacuoles in *gop-1(tm5384)* coelomocytes were labeled by both RME-8::GFP, the endosome marker, and LMP-1::GFP, a lysosomal membrane protein, suggesting that they are aberrant endosome/lysosome hybrids (Fig. 7, A–C′, E–G′, I, and J). Identical phenotypes were observed in *unc-108;gop-1* double mutants (Fig. 7, D–D′, H–H′, I, and J). Texas red–conjugated BSA (TR-BSA), which was taken up by wild-type coelomocytes and transported to lysosomes within 30 min of injection into the body cavity, was trapped in the large vacuoles in *gop-1(tm5384)* coelomocytes, a phenotype resembling that of *unc-108* mutants (Fig. S4, A and B; Lu et al., 2008). These data suggest that GOP-1 promotes endosome maturation like UNC-108.

UNC-108 regulates DCV maturation by preventing specific cargo from entering the late endosome system and therefore retaining them in the mature DCV (Edwards et al., 2009; Sumakovic et al., 2009). We found that loss of *gop-1* led to greatly reduced NLP-21::VENUS, a soluble DCV cargo, and IDA-1::GFP, a DCV-specific membrane protein, in neuron axons and the appearance of big NLP-21::VENUS vesicles in neuron cell bodies, phenotypes that were indistinguishable from those of *unc-108(lf)* single mutants or *unc-108;gop-1* double mutants (Fig. 7, K–T; and Fig. S4, C–G). In addition, loss of *gop-1* caused increased GLR-1::GFP in the ventral nerve cord like *unc-108(lf)* and *unc-108;gop-1*, suggesting that GOP-1 also plays a role in trafficking of the glutamate receptor GLR-1 like UNC-108 (Fig. S4, H–L; Chun et al., 2008). Consistent with defects in DCV maturation and GLR-1 trafficking, *gop-1(tm5384)* mutants displayed an uncoordinated locomotion phenotype similar to *unc-108(3263)* single mutants and *unc-108;gop-1* double mutants (Fig. S2 I). These data indicate that GOP-1 acts in the same pathway with UNC-108 to promote endosome and DCV maturation. Expression of human *CLEC16A* efficiently rescued the endosome maturation and locomotion defects of *gop-1(tm5384)*, indicating that CLEC16A can replace GOP-1 in these processes (Fig. S2, F, H, and I).

As on phagosomes, UNC-108 appeared transiently on endosomes for ∼9.3 min in wild-type coelomocytes (Video 7 and Fig. 8 A). UNC-108 release coincided with or immediately followed the appearance of the lysosomal marker NUC-1, consistent with the role of UNC-108 in endosome maturation (Fig. 8 A). In *gop-1(tm5384)* mutants, however, endosomal recruitment of UNC-108 was abrogated (Video 8 and Fig. 8 B). In contrast, GOP-1::GFP associated with endosomes in both wild-type and *unc-108(lf)* coelomocytes (Fig. 8, C–E). These data indicate that GOP-1 is required to recruit UNC-108 to endosomes, whereas UNC-108 is dispensable for endosomal association of GOP-1.

GOP-1 interacts with GDP-bound and nucleotide-free UNC-108

Next, we determined whether GOP-1 physically interacts with UNC-108. GOP-1 interacted with UNC-108 but not RAB-5, RAB-7, or RAB-14 in yeast two-hybrid assays, suggesting that GOP-1 is a specific binding partner of UNC-108 (Figs. 9 A and S5 A). Using various mutant forms of UNC-108 that fix the Rab in different nucleotide-binding states, we found that GOP-1 interacted with GDP-bound UNC-108(S20N) and the nucleotide-free mutant of UNC-108(N119I), but not wild-type or GTP-bound UNC-108(Q65L) (Fig. 9 A). Consistent with this, significantly more HIS-tagged GOP-1 was pulled down by GST-UNC-108(S20N) and GST-UNC-108(N119I) than wild-type UNC-108 or UNC-108(Q65L) (Fig. 9 B). These data indicate that GOP-1 interacts specifically with the inactive GDP-bound and nucleotide-free UNC-108, consistent with its role in membrane recruitment and activation of UNC-108. All GOP-1–positive phagosomes contained UNC-108, and GFP::GOP-1 coprecipitated with Cherry::UNC-108 in worms expressing both proteins, indicating that GOP-1 associates with UNC-108 in vivo (Fig. 9, C–D′′′).

GOP-1 disrupts UNC-108–GDI-1 complexes and promotes activation of UNC-108

The activation of Rab proteins requires dissociation of Rab from the GDI–Rab complex, followed by GEF-catalyzed nucleotide exchange. We purified GDI-1–UNC-108 complexes from yeast cells in which Rabs can be prenylated (Fig. S5 B). Wild-type UNC-108 but not UNC-108 (ΔCC), which lacks the two prenylatable C-terminal cysteines, associated with GDI-1, suggesting that UNC-108 in complex with GDI-1 is prenylated (Figs. S2 J and S5 C; Musha et al., 1992; Farnsworth et al., 1994). We incubated the GDI-1–UNC-108 complex with GOP-1 immobilized on GST beads and found that UNC-108 bound strongly to GST-GOP-1 but not GST-only beads, whereas GDI-1 remained in the supernatant (Fig. 9 E). When purified UNC-108–GDI-1 was immobilized on magnetic beads and incubated with soluble GOP-1, GOP-1 was coprecipitated with the UNC-108–coated magnetic beads, whereas the association of GDI-1 with the beads was reduced (Fig. S5 D). These data suggest that GOP-1 disrupts the Rab–GDI complex, causing dissociation of UNC-108 from GDI-1. Next, to examine whether GOP-1 promotes membrane recruitment of UNC-108, we performed a flotation assay using PC liposomes containing PtdIns3P to mimic PtdIns3P-positive phagosomes (Fig. 10 A). Incubation of GOP-1 with UNC-108–GDI-1 led to association of UNC-108 but not GDI-1 with PC + PtdIns3P liposomes, and this was enhanced by addition of GTPγS, which prevents GTP hydrolysis (Fig. 10 A). Recombinant GOP-1 or UNC-108 by itself, however, did not associate with liposomes (Fig. S5, E and F). We found that GOP-1 strongly facilitated loading of GTPγS onto UNC-108 when incubated with UNC-108–GDI-1 in the presence of ^{35}S-labeled GTPγS (Fig. 10 B). Collectively, these data suggest that GOP-1 promotes activation and membrane association of UNC-108. To further examine this, we mutated lysine 120, which resides in the highly conserved guanine base-binding motif, in UNC-108 (Fig. S2 J; Pereira-Leal and Seabra, 2000). The analogous mutation in Ypt7, which weakens the affinity for the nucleotide and thus facilitates nucleotide exchange, bypasses the necessity for its GEF (Kucharczyk et al., 2001; Cabrera and Ungermann, 2013). We found that K120E, but not wild-type UNC-108, associated with phagosomes and endosomes in the absence of GOP-1 (Fig. 10, C–G). Moreover, expression of UNC-108(K120E) rescued the germ-cell corpse phenotype and partially reversed the endosome maturation

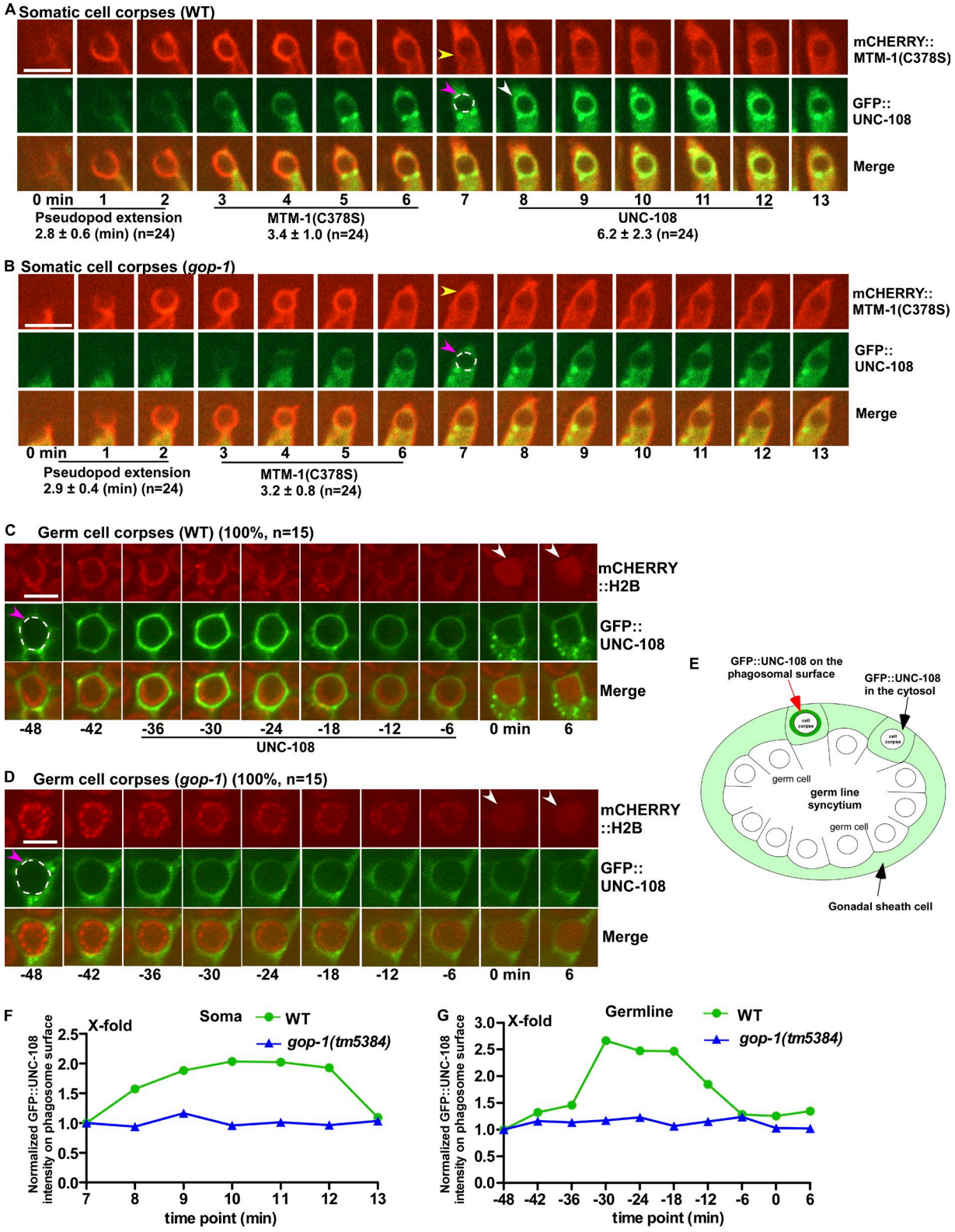

Figure 6. **Loss of *gop-1* affects phagosomal recruitment of UNC-108.** (A and B) Time-lapse images of somatic cell corpses in wild type (WT; A) and *gop-1(tm5384)* (B) expressing mCherry::MTM-1(C378S) and GFP::UNC-108. 0 min, time point when MTM-1(C378S) was first detected around the cell corpse. The time period until the cell corpse was surrounded by MTM-1(C378S) was defined as the pseudopod extension stage. Quantification of pseudopod extension and the phagosomal duration of MTM-1 and UNC-108 is shown at bottom (mean ± SD). *n*, number of phagosomes quantified. Yellow arrowheads, MTM-1 release from phagosomes; white arrowhead, recruitment of GFP::UNC-108 to the phagosomal membrane. (C and D) Time-lapse images of germ cell corpses in wild type (WT; C) and *gop-1(tm5384)* (D) expressing GFP::UNC-108 and mCherry::H2B (Histone 2B). 0 min, time point when phagosomal degradation of the apoptotic cell, indicated by diffuse H2B (white arrowheads), was observed. In wild type, UNC-108 was enriched on the phagosomal membrane 36 min before diffuse H2B was observed, whereas it was absent from phagosomes in *gop-1(tm5384)*. Percentage of phagosomes with the

defect in *gop-1(tm5384)* mutants, consistent with GOP-1 acting as an activator of UNC-108 (Fig. S2, A, G, and H).

Discussion

GOP-1 and UNC-108/Rab2 act in parallel with TBC-2 and SAND-1/Mon1 to promote phagosome progression through the RAB-5–positive stage

We identified *gop-1* as a novel regulator of apoptotic cell clearance that promotes phagosome maturation by activating UNC-108/Rab2. GOP-1 transiently associates with apoptotic cell–containing phagosomes, a process that requires RAB-5 function and may be facilitated by membrane PtdIns3P. Because GOP-1 did not interact with RAB-5 or associate with PtdIn3P (Fig. S5, A and E), its recruitment to phagosomes may be mediated by effectors of RAB-5 or PtdIns3P. UNC-108/Rab2 is recruited to apoptotic cell–containing phagosomes by GOP-1, which promotes UNC-108 activation and thus stabilizes the Rab on the phagosomal surface. Our data suggest that GOP-1–UNC-108 promotes phagosome progression from the RAB-5–positive stage to the RAB-7–positive stage, a process that also involves TBC-2–mediated RAB-5 inactivation and SAND-1–mediated RAB-7 recruitment (Li et al., 2009; Kinchen and Ravichandran, 2010). We found that loss of *tbc-2* and *sand-1* significantly enhanced the persistent cell corpse and phagosome maturation phenotypes in *gop-1(lf)* and *unc-108(lf)* mutants, suggesting that parallel mechanisms are involved. Consistent with this, GOP-1 and UNC-108 do not associate with TBC-2 or affect its recruitment to phagosomes (unpublished data). Thus, multiple mechanisms are engaged to control phagosome maturation through the RAB-5–positive stage. Future work should identify UNC-108/Rab2 effectors and reveal the UNC-108/Rab2-dependent mechanism in this process.

GOP-1 promotes UNC-108/Rab2 activation in multiple processes

UNC-108 regulates multiple processes including apoptotic cell degradation and endosome and DCV maturation, whereas mammalian Rab2 controls protein secretion and recycling through the Golgi apparatus. How Rab2 is targeted to and activated on the specific membrane compartment in these processes remains unknown. Here we present five lines of evidence that GOP-1 is an upstream activator of UNC-108/Rab2. First, *unc-108* and *gop-1* mutants exhibit identical phenotypes in apoptotic cell removal and maturation of endosomes and DCVs; these defects are unaltered in *unc-108;gop-1* double mutants, indicating that GOP-1 acts together with UNC-108 in all three processes. Second, loss of GOP-1 disrupts phagosomal and endosomal association of UNC-108, whereas UNC-108 is dispensable for recruiting GOP-1 to membranes. Third, GOP-1 binds to the inactive GDP-bound and nucleotide-free UNC-108, but not the active GTP-bound UNC-108. Fourth, GOP-1 disrupts UNC-108–GDI-1 complexes and promotes GTP loading onto and membrane association of UNC-108. Fifth, mutation of lysine 120 of UNC-108, which resides in the conserved guanine base–contacting motif and may facilitate nucleotide exchange, bypasses the necessity for GOP-1 in cell corpse removal and endosome maturation. Thus, GOP-1 promotes UNC-108 activation in multiple processes.

Rab activation requires its disassociation from the Rab–GDI complex and subsequent nucleotide exchange catalyzed by GEF. We found that GOP-1 disrupts UNC-108–GDI-1 complexes and promotes loading of GTP onto and membrane association of UNC-108 by using Rab–GDI as the substrate. GOP-1 binds strongly to the nucleotide-free form of UNC-108, a hallmark of GEF; loss of GOP-1 completely disrupts phagosomal and endosomal targeting of UNC-108, whereas UNC-108(K120E), a mutation that may facilitate nucleotide exchange of Rab, reverses the membrane targeting defect of UNC-108 in *gop-1* mutants. Together, these data suggest that GOP-1 may act as a GEF of UNC-108 that serves both GDI displacement and nucleotide exchange functions. However, by in vitro GEF assays, we failed to detect GEF activity of GOP-1 toward UNC-108 (unprenylated or prenylated) in the presence or absence of liposomes. Notably, many GEFs, including those of Ras, Ran, Rho, Arf, and Rab, are regulated through autoinhibitory mechanisms (Cherfils and Zeghouf, 2013). For example, RABEX-5, the RAB5 GEF, forms a complex with RABAPTIN-5, an effector of RAB5 that suppresses the autoinhibition of RABEX-5 (Horiuchi et al., 1997; Delprato and Lambright, 2007). We suspect that the nucleotide exchange activity of GOP-1 may be regulated in vivo by additional modifications, cofactors, or autoinhibitory elements and is thus not revealed in vitro by recombinant GOP-1. Further work, especially structural studies of GOP-1, should clarify this issue.

Activation of Rab GTPase 2 by GOP-1 may be evolutionarily conserved

GOP-1 shares sequence homology with *Drosophila* Ema and human CLEC16A, both of which associate with endolysosomal compartments and/or the Golgi complex, like GOP-1, and are implicated in endosomal maturation and autophagosomal trafficking (Kim et al., 2010, 2012; Soleimanpour et al., 2014; van Luijn et al., 2015). These findings indicate conserved functions of this gene family in membrane trafficking, a process extensively regulated by Rab GTPases. Our data indicate that GOP-1 promotes activation of Rab GTPase 2 in multiple processes. Moreover, expression of CLEC16A in worms efficiently rescues the persistent cell corpse, endosomal maturation, and locomotion phenotypes of *gop-1(lf)* mutants, indicating that CLEC16A can substitute for GOP-1 in all these processes. Thus, GOP-1 family proteins may serve as a novel family of Rab activators to regulate multiple membrane trafficking

representative pattern is shown in parentheses. *n*, number of phagosomes that were followed and quantified. In A–D, pink arrowheads indicate the first time point when the intensity of GFP::UNC-108 on the phagosomal surface (white dashed line) was measured. Bars, 5 µm. (E) Cartoon showing a cross section of a pair of gonadal sheath cells expressing GFP::UNC-108. Two apoptotic germ cells engulfed by sheath cells are shown. Red arrow, appearance of GFP::UNC-108 on the phagosomal surface (dark green); black arrows, diffuse GFP::UNC-108 in the sheath cell cytosol (light green) separated by germ cell nuclei. (F and G) Total fluorescence intensity of GFP::UNC-108 on the phagosomal surface in embryos (F) or germ line (G) at different time points as shown in A–D was measured, and the normalized fluorescence intensity is shown. Enrichment of GFP::UNC-108 on the phagosomal surface was seen in wild type but not *gop-1(tm5384)* mutants.

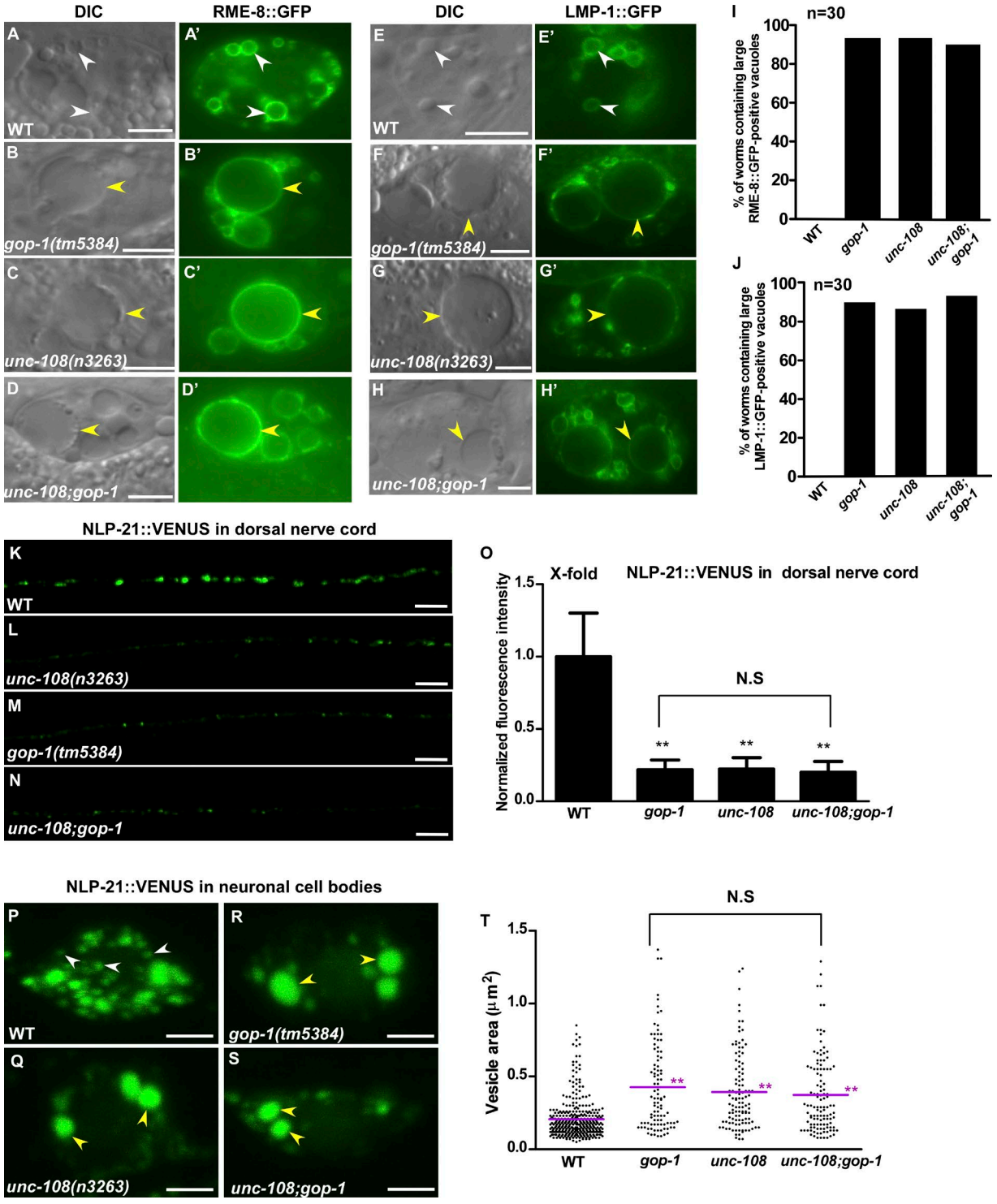

Figure 7. **Loss of *gop-1* affects endosome and dense core vesicle maturation.** (A–J) DIC and fluorescent images of coelomocytes expressing RME-8::GFP (A–D′) or LMP-1::GFP (E–H′) in the indicated strains. RME-8::GFP and LMP-1::GFP associate with endosomes and lysosomes, respectively, in wild type (white arrowheads), but label enlarged vacuoles (yellow arrowheads) in *gop-1(tm5384)*, *unc-108(n3263)*, and *unc-108;gop-1* worms. Quantification is shown in I and J. At least 30 animals were scored in each strain. (K–O) Confocal fluorescence images of the dorsal nerve cord in the indicated strains expressing NLP-21::VENUS (K–N). Quantification is shown in O. At least 30 animals were scored in each strain. Data are shown as mean ± SD. One-way ANOVA with Tukey's posttest was performed to compare mutant datasets with wild type or datasets linked by lines. **, $P < 0.0001$; N.S., no significance. (P–T) Confocal fluorescence images of the neuronal cell body in the ventral nerve cord expressing NLP-21::VENUS in the indicated strains. White arrowheads, small vesicles (<0.4 μm²); yellow arrowheads, large ones (>0.8 μm²). The surface area of NLP-21–positive vesicles in neuronal bodies was quantified in the indicated strains, and the size distribution of vesicles is shown in T. Purple lines indicate the mean surface area. At least 15 animals were scored in each strain. One-way ANOVA with Tukey's posttest was performed to compare mutant datasets with wild type or datasets linked by lines. **, $P < 0.0001$; N.S., no significance. Bars: (A–H′ and K–N) 5 μm; (P–S) 2 μm.

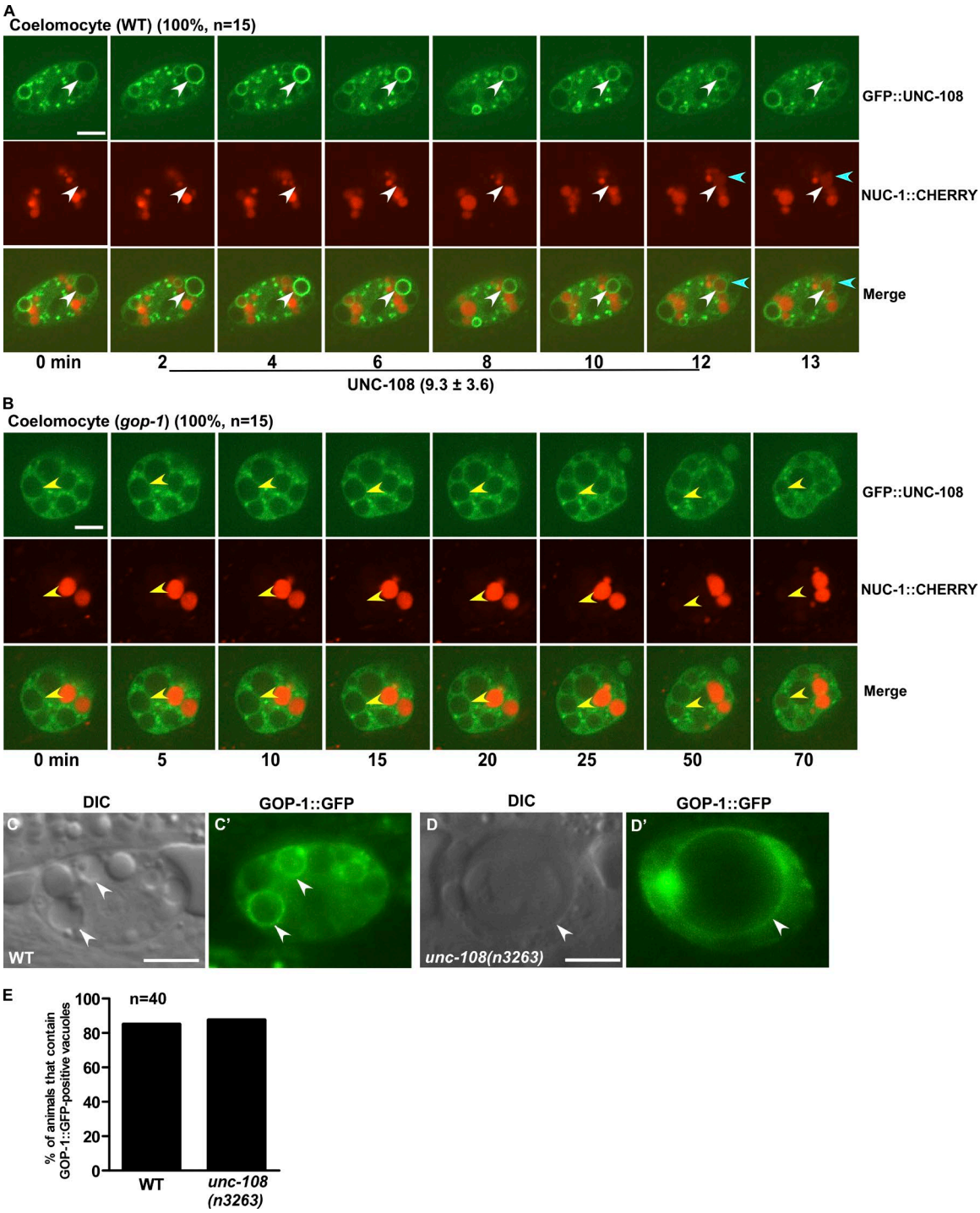

Figure 8. **Loss of *gop-1* disrupts endosomal recruitment of UNC-108.** (A and B) Time-lapse images of coelomocytes in wild type (WT; A) and *gop-1(tm5384)* (B) expressing GFP::UNC-108 and NUC-1::Cherry. 0 min, time point before GFP::UNC-108 was initially detected on endosomes. White arrowheads, recruitment of GFP::UNC-108 to the endosome membrane; blue arrowheads, appearance of NUC-1::Cherry; yellow arrowheads, absence of UNC-108 from endosomes in *gop-1(tm5384)*. The duration of UNC-108 on endosomes was quantified and is shown beneath the images (mean ± SD). *n*, number of endosomes quantified. (C and D) DIC and fluorescent images of coelomocytes in wild type (WT; C and C') and *gop-1(tm5384)* (D and D') expressing GOP-1::GFP. White arrowheads, GOP-1::GFP-positive vesicles. (E) Percentage of animals that contain GOP-1::GFP-positive vacuoles in coelomocytes was quantified and is shown. *n*, number of worms that were quantified. Bars, 5 µm.

events. In genome-wide association studies, *CLEC16A* is associated with several autoimmune diseases such as type 1 diabetes mellitus, multiple sclerosis, and primary adrenal insufficiency, but how its deficiency contributes to disease pathogenesis remains largely unknown (Hakonarson et al., 2007; Skinningsrud et al., 2008; Hoppenbrouwers et al., 2009; Márquez et al., 2009). Our findings reveal the essential role of GOP-1 in the activation of Rab GTPase 2, which may contribute to the pathogenesis of diseases associated with *CLEC16A* deficiency.

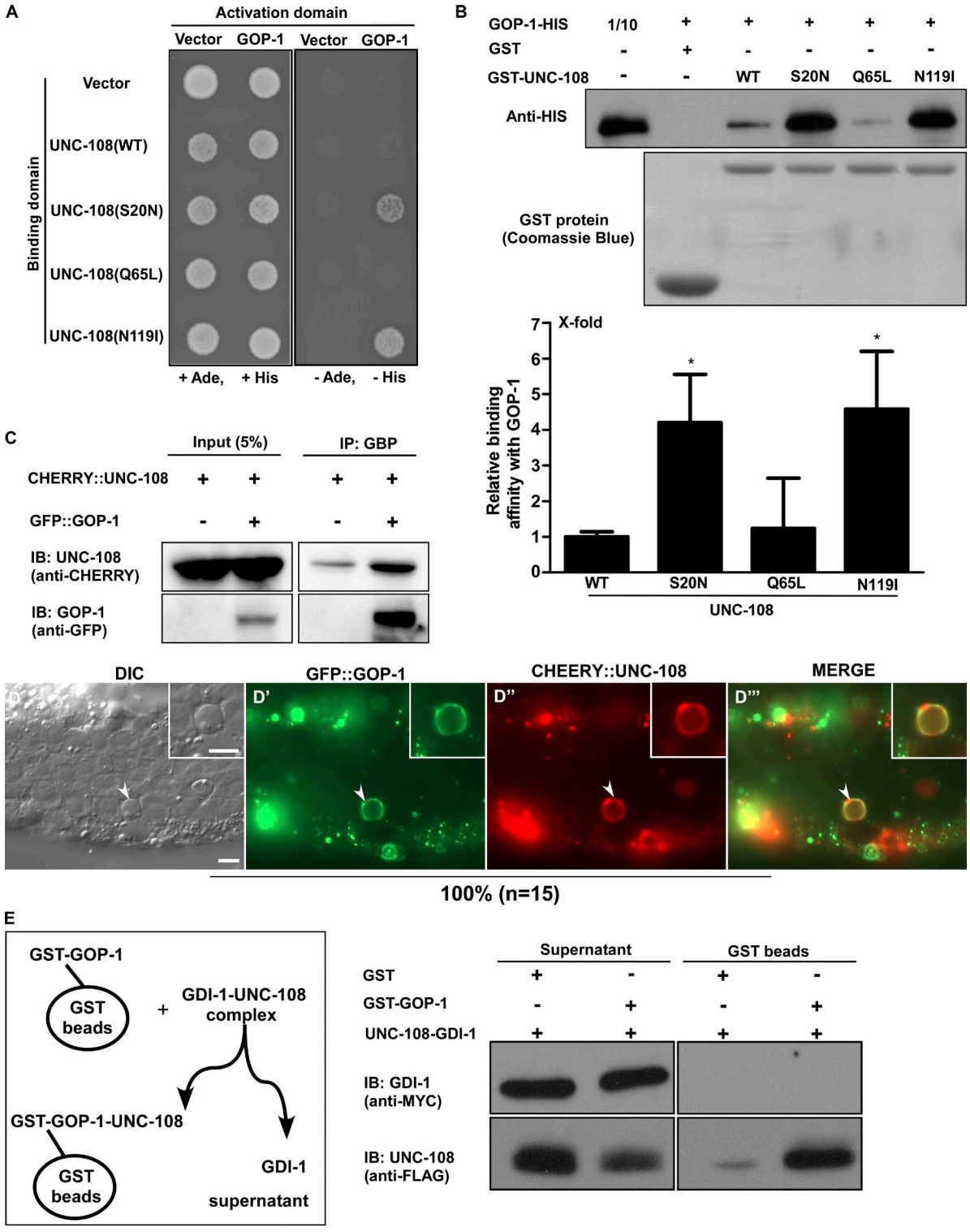

Figure 9. **GOP-1 interacts with UNC-108 and disrupts the UNC-108–GDI-1 complex.** (A and B) The interaction between GOP-1 and UNC-108 was examined by yeast two-hybrid analyses (Y2H; A) and GST pull-down assays (B). GOP-1 specifically interacts with the GDP-bound and nucleotide-free forms of UNC-108 in Y2H (A), whereas significantly more GOP-1-HIS is pulled down by GST-UNC-108(S20N) (GDP-bound) and GST-UNC-108(N119I) (nucleotide-free) than by GST-UNC108(WT) and GST-UNC-108(Q65L) (GTP-bound; B). At least four independent experiments were performed, and data are shown as mean ± SD. One-way ANOVA with Tukey's posttest was performed to compare mutant datasets with wild type. *, $P < 0.05$; N.S., no significance. (C) Cherry::UNC-108 is coprecipitated with GFP::GOP-1 by GBP pull-down in lysates prepared from adult worms coexpressing both fusion proteins. (D–D‴) DIC and fluorescent images of the wild-type germ line coexpressing GFP::GOP-1 and Cherry::UNC-108. GOP-1 and UNC-108 colocalized on the phagosome (arrowheads). *n*, number of worms quantified. Bars, 5 µm. (E) GOP-1 disrupts the UNC-108–GDI-1 complex. Schematic illustration of the GDI displacement assay is shown at left. Addition of GST-GOP-1 but not GST led to association of UNC-108 but not GDI-1 with GST-beads. At least three independent experiments were performed, and a representative result is shown.

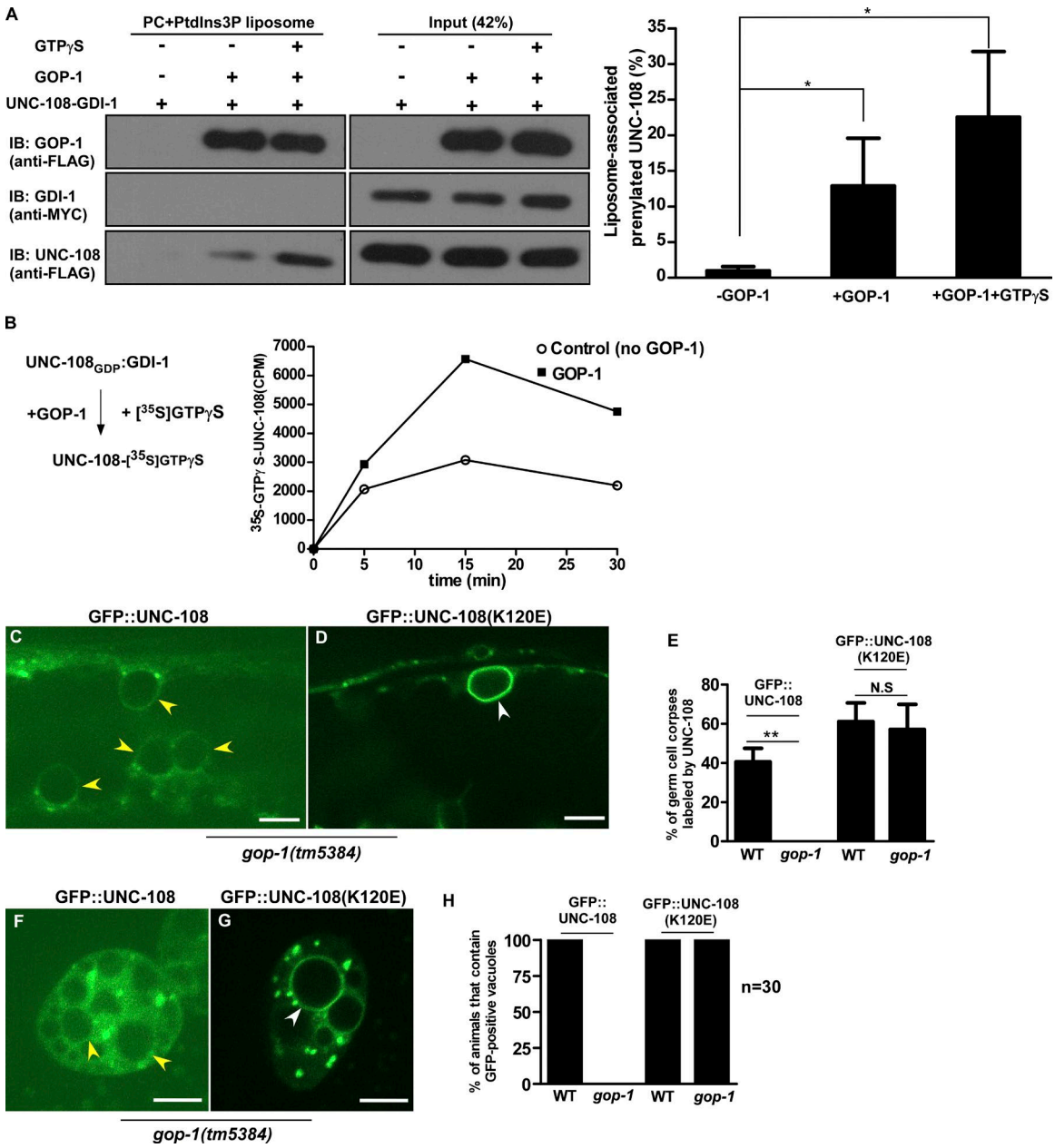

Figure 10. **GOP-1 promotes loading of GTP onto and membrane recruitment of UNC-108.** GOP-1 promotes association of UNC-108 with liposomes. Binding of UNC-108–GDI-1 to PC + PtdIns3P (8%) liposomes was detected by Western blot. UNC-108 but not GDI-1 was recovered in the top fraction with GOP-1 in a liposome flotation assay in the absence or presence of GTPγS. Quantification is shown at right. At least three independent experiments were performed. Data are shown as mean ± SD. Unpaired *t* test was performed to compare datasets linked by lines. *, $P < 0.05$. (B) GOP-1 promotes loading of GTP onto UNC-108. Schematic illustration of the GTP incorporation assay is shown at left. At least three independent experiments were performed, and a representative result is shown. (C–H) Fluorescent images of the gonads (C and D) or coelomocytes (F and G) in *gop-1(tm5384)* expressing GFP::UNC-108 (C and F) or GFP::UNC-108(K120E) (D and G). K120E (white arrowheads) but not wild-type UNC-108 (yellow arrowheads) was seen on phagosomes (C and D) and endosomes (F and G). Quantification is shown in E and H. In E, at least 15 animals were scored, and data are shown as mean ± SD. Unpaired *t* test was performed to compare data derived from wild type and *gop-1(tm5384)*. **, $P < 0.0001$; N.S., no significant difference. In H, the percentage of animals containing GFP-positive vacuoles in coelomocytes was quantified. *n*, number of animals followed and quantified. Bars, 5 µm.

Materials and methods

C. elegans strains

Strains of *C. elegans* were cultured and maintained using standard protocols. The N2 Bristol strain was used as the wild-type strain. The following strains were used in this work: linkage group I (LG I), *unc-108(n3263)*; LG II, *tbc-2(qx20)*; LG III, *gop-1(tm5384*, *tm5654*, *tm5694*, *yq79)*; LG IV, *sand-1(ok1963)*; LG V, *unc-76(e911)*; and LG X, *rab-14(tm2095)*.

Standard microinjection methods were used to generate transgenic animals carrying extrachromosomal arrays (*qxEx*), and genome-integrated arrays (*qxIs*) were acquired by γ-ray irradiation to achieve stable expression from arrays with low copy numbers. The reporter strains used in this study are as follows: *smIs76* (P_{hsp}Annexin-V::GFP), *qxIs477* ($P_{ced\text{-}1}$mCherry::MTM-1(C378S)), *qxIs408* ($P_{ced\text{-}1}$GFP::RAB-5), *qxIs456* ($P_{ced\text{-}1}$mCherry::RAB-5), *qxIs66* ($P_{ced\text{-}1}$GFP::RAB-7), *qxIs68* ($P_{ced\text{-}1}$mCherry::RAB-7), *qxIs234* ($P_{ced\text{-}1}$GFP::UNC-108),

qxIs466 ($P_{ced\text{-}1}$mCherry::UNC-108), *qxIs257* ($P_{ced\text{-}1}$NUC-1::nCherry), *qxIs390* ($P_{ced\text{-}1}$myriGFP), *qxIs458* ($P_{ced\text{-}1}$GFP::GOP-1), *qxEx4387* ($P_{gop\text{-}1}$GOP-1::GFP), *qxIs354* ($P_{ced\text{-}1}$LAAT-1::GFP), *smIs34* ($P_{ced\text{-}1}$CED-1::GFP), *qxEx4320* ($P_{gop\text{-}1}$GFP), *qxEx6226* ($P_{ced\text{-}1}$CLEC16A-FLAG), *qxEx7115* ($P_{ced\text{-}1}$GFP::UNC-108(K120E)), *qxEx711*8 ($P_{unc\text{-}122}$GFP::UNC-108(K120E)), *qxEx7264* ($P_{gop\text{-}1}$CLEC16A-FLAG), *qxEx5088* ($P_{ced\text{-}1}$GFP::GOP-1+$P_{ced\text{-}1}$mCherry::FAPP1-PH), *qxEx5638* ($P_{ced\text{-}1}$GFP::UNC-108+$P_{ced\text{-}1}$mCherry::FAPP1-PH), *qxEx5199* ($P_{ced\text{-}1}$GFP::GOP-1+$P_{ced\text{-}1}$mCherry::TRAM-1), and *qxEx5636* ($P_{unc\text{-}122}$GFP::UNC-108).

We obtained *opIs334* ($P_{ced\text{-}1}$YFP::2xFYVE) from K.S. Ravichandran (University of Virginia, Charlottesville, VA) and M.O. Hengartner (University of Zurich, Zurich, Switzerland); *ceIs72* ($P_{unc\text{-}129}$IDA-1::GFP) from K.G. Miller (Oklahoma Medical Research Foundation, Oklahoma City, OK); *nuIs183* ($P_{unc\text{-}129}$NLP-21::Venus) and *nuIs24* ($P_{glr\text{-}1}$GLR-1::GFP) from J.M. Kaplan (Massachusetts General Hospital, Boston, MA); *bIs34* (P_{cc1}RME-8::GFP) from H. Fares (University of Arizona, Tucson, AZ); *pwIs50* (LMP-1::GFP) from B. Grant (Rutgers University, New Brunswick, NJ); and *itIs37* ($P_{pie\text{-}1}$mCherry::H2B) from Z. Bao (Sloan Kettering Institute, New York, NY).

Yeast strain

Yeast strain BCY123 (*MATa*, *Can1*, *ade2*, *trp1*, *Ura3-52*, *his3*, *leu2-3*, *112, pep4::his*$^+$, *prb1::leu2*$^+$, *bar1::HisG*$^+$, and *lys2::pGAL1/10-GAL4*$^+$) was provided by J. Zhou (Institute of Biochemistry and Cell Biology, Shanghai Institutes for Biological Sciences, Shanghai, China).

Isolation of *gop-1* deletion alleles

gop-1 deletion alleles were isolated from a trimethylpsoralen and ultraviolet-mutagenized library, as described previously (Gengyo-Ando and Mitani, 2000). *gop-1* mutant alleles were identified by nested PCR with the following primers: 5′-TGGGTCACTATGGAAGCCGA-3′ and 5′-GCTACGCATGTGTCCCTTTA-3′ as first-round primers and 5′-AAG CATTACGAGCTATCGCA-3′ and 5′-CTTACTGTCTGAAGAGGA GT-3′ as second-round primers for *tm5384* and *tm5694*, or 5′-GCG TAGCTTGTTGTGTGGGT-3′ and 5′-CGTGCTGTTTGGCGACCC TA-3′ as first-round primers and 5′-CTCGCCGCGCTTTGTTTGAT-3′ and 5′-CGTTACCTTGGTGAGCCGTT-3′ as second-round primers for *tm5654*. The *yq79* mutation was isolated from a forward genetic screen for additional regulators of cell corpse clearance. *yq79* was mapped to the left arm of LG III between genetic map positions −3.79 (Snp-WBVar00058951) and −1.57 (Snp-WBVar00060777) by single nucleotide polymorphism mapping. The complementation test indicated that *yq79* and *tm5384* affected the same gene. The sequence of the *gop-1* gene was determined in all *gop-1* alleles. The *tm5384* deletion allele contains a 511-bp deletion that causes a frame shift after Tyr 111, resulting in an early stop codon after Ile 134. The *tm5654* allele of *gop-1* contains a 1,185-bp deletion that removes most of exon 8, all of exons 9–13, and part of exon 14, resulting in a frame shift after Val 698. The *tm5694* allele of *gop-1* contains a 739-bp deletion that removes part of exon 3, all of exons 4 and 5, and part of exon 6, resulting in a truncated protein lacking aa 140–340. *yq79* contains a C-to-T mutation that causes a premature stop codon after Arg 49. All mutants were backcrossed with N2 animals at least four times before further analyses.

Quantification of cell corpses, cell death events, cell corpse duration, and phagosome maturation

The number of somatic cell corpses in the head region of living embryos and the number of germ cell corpses in one gonad arm at various adult ages were scored as described (Gumienny et al., 1999; Wang et al., 2002). The cell corpses were identified by their raised button–like morphology using Nomarski optics. At least 15 animals were scored at each stage in each strain. To examine embryonic cell deaths and cell corpse duration, embryos at the two-cell stage (cell death occurrence) or precomma stage (embryonic cell copse duration) or adult animals (24 h after L4/adult molt, germ cell corpse duration) were mounted on agar pads. Images in 40 *z*-sections (1.0 µm/section, cell death occurrence) or 30 *z*-series (1.0 µm/section, cell corpse duration) were captured every 2 min for 8 h (cell death occurrence) or 2–4 h (cell corpse duration) using an Axioimager M1 microscope (ZEISS) equipped with an AxioCam monochrome digital camera (ZEISS). Images were processed and viewed using Axiovision Rel 4.7 software (ZEISS).

To examine phagosome maturation, differential interference contrast (DIC) and fluorescence images were captured using an Axioimager A1 microscope (ZEISS) as described before (Lu et al., 2008). The percentage of somatic and germ cell corpses labeled by various phagosomal markers was quantified in embryos at the 1.5-fold stage or adult animals (24 or 48 h after L4/adult molt) by dividing the total number of cell corpses by the number of labeled ones. Corpses were examined at multiple focal planes. At least 15 animals were scored in each strain.

Microscopy and imaging analysis

DIC and fluorescent images were captured with an Axioimager A1 equipped with epifluorescence (Filter Set 13 for GFP [excitation, BP 470/20; beam splitter, FT 495; emission, BP 503–530] and Filter Set 20 for Cherry [excitation, BP 546/12; beam splitter, FT 560; emission, BP 575–640]) and an AxioCam monochrome digital camera. Images were processed and viewed using Axiovision Rel. 4.7 software. A 100× Plan-Neofluar objective (NA 1.30) was used with Immersol 518F oil (ZEISS). For confocal images, a ZEISS LSM 5 Pascal inverted confocal microscope with 488 (emission filter, BP 503–530) and 543 (emission filter, BP 560–615) lasers was used, and images were processed and viewed using LSM Image Browser software (ZEISS). All images were taken at 20°C.

Spinning-disk time-lapse recording

The dynamic association of MTM-1::Cherry(C378S), GFP::UNC-108, GFP::RAB-5, YFP::2xFYVE, GFP::RAB-7, LAAT-1::GFP, and NUC-1::Cherry with phagosomal or endosomal membranes was recorded by spinning-disk time-lapse recording as described previously (Cheng et al., 2015). In brief, adult animals (24–36 h after L4/adult molt) or embryos at the precomma stage were mounted on agar pads in M9 buffer in the presence (adult worms) or absence (embryos) of 5 mM levamisole to prevent animals from moving without affecting the germline or the gonad. Fluorescent images were captured using a 100× objective (NA 1.45) with immersion oil (Type NF) on an inverted fluorescence microscope (Nikon Eclipse Ti-E) with an UltraView spinning-disc confocal scanner unit (PerkinElmer) with 488 (emission filter 525 [W50]) and 561 (dual-band emission filter 445 [W60] and 615 [W70]) lasers. Images in 15–20 *z*-sections (1.0 µm/section) were captured every 1 min for 2 h (embryos), 2–5 h (adult animals), or 2–3 h (coelomocytes in adult animals) at 20°C. Volocity software (PerkinElmer) was used to view and analyze images. The numbers of phagosomes or endosomes that were followed and quantified are indicated in the figures and figure legends.

Endocytosis assay

In vivo pulse-chase experiments were performed as described (Zhang et al., 2001). In brief, TR-BSA was injected into the body cavity in the pharyngeal region at 1 mg/ml. Injected worms were transferred to seeded NGM plates at RT, and the uptake by coelomocytes was recorded at the indicated time points (5, 15, 30, and 60 min). At each time point, the injected worms were transferred to an ice-cold NGM plate to stop the intracellular trafficking of endocytosed molecules before examination by epifluorescence microscopy.

Examination of dense core vesicle cargo and GLR-1::GFP

Live animals (12 h after L4/adult molt) expressing NLP-21::VENUS, IDA-1::GFP, or GLR-1::GFP were mounted on agar pads in M9 in the presence of 5 mM levamisole. All images were taken with equal exposure time with an LSM 5 Pascal inverted confocal microscope (ZEISS) with the 488 laser (emission filter, BP 503–530). Images were processed and viewed using LSM Image Browser software. To examine NLP-21::VENUS, IDA-1::GFP, and GLR-1::GFP patterns, the posterior region of the dorsal nerve cord (NLP-21, IDA-1) or ventral nerve cord (GLR-1) was oriented toward the objective as described (Sumakovic et al., 2009). Images in five *z*-series (1.0 µm/section) were captured. Maximum stack projections of images were obtained using LSM Image Browser, and the fluorescence intensity was measured by ImageJ and normalized to wild type. To examine NLP-21::VENUS in neuronal cell bodies in ventral nerve cord, images of entire cell bodies were captured in eight *z*-series (1.0 µm/section). The diameter of each NLP-21::VENUS–positive vesicle was quantified using ImageJ.

Lysosensor green staining

Lysosensor green staining was performed as described before (Guo et al., 2010). In brief, adult worms (48 h after L4/adult molt) were dissected in gonad dissection buffer (60 mM NaCl, 32 mM KCl, 3 mM Na_2HPO_4, 2 mM $MgCl_2$, 20 mM Hepes, 50 µg/ml penicillin, 50 µg/ml streptomycin, 100 µg/ml neomycin, 10 mM glucose, 33% FCS, and 2 mM $CaCl_2$) with 1 µM Lysosensor green DND-189 (Invitrogen) and examined by fluorescence microscopy.

Locomotion assay

The locomotion assay was performed as described before (Sumakovic et al., 2009). Adult animals were transferred to unseeded NGM plates to give an initial adjustment period of 60 min. Locomotion was then assayed by counting the number of body bends (corresponding to a whole 360° sine wave) in a period of 3 min.

RNAi

The bacteria feeding protocol was used in RNAi experiments. In each experiment, L4 larvae (P0) were cultured on the RNAi plates. The F1 progeny at the L4 stage were transferred to fresh RNAi plates and aged for 48 h before examination of germ cell corpses. Embryonic cell corpses were scored in the F2 progeny. For *rab-5* RNAi, 30 L2 or L3 larvae (P0) were cultured on the RNAi plates, and germ cell corpses were scored 48 h after L4/adult molt at the same generation because most F1 progeny die before reaching the adult stage as a result of inactivation of *rab-5*. To quantify somatic cell corpses in *rab-5* RNAi worms, L4 larvae (P0) were cultured on the RNAi plates, and cell corpses were examined in the F1 embryos. The DNA sequences that are targeted by the dsRNAs in the RNAi experiments are as follows: *rab-7* (W03C9, 32,688–34,320 nt), *rab-5* (F26H9, 20,787–22,312 nt), *unc-108* (F53F10, 9,645–10,724 nt), and *gop-1* (C34E10, 27,648–28,758 nt).

Yeast two-hybrid assays

Yeast two-hybrid analyses were performed using the Matchmaker yeast two-hybrid system according to the manufacturer's instructions (Takara Bio, Inc.). Specific cDNAs to be tested were cloned into the pGADT7 and pGBKT7 vectors to produce Gal4 transcription activation domain (AD) and DNA binding domain (BD) fusion proteins. Specific pairs of constructs expressing AD and BD fusion proteins were transformed into the yeast strain AH109, and transformants were selected on synthetic complete (SC) medium lacking leucine and tryptophan (SC-Leu-Trp). Individual clones were streaked on SC-Ade-His–Leu-Trp plates to test for the activation of the reporter genes *HIS3* and *ADE2*. Self-interaction of GOP-1 or UNC-108 was also tested.

Expression and purification of recombinant proteins

Full-length cDNA of *unc-108* (WT/S20N/Q65L/N119I) and *gop-1* was cloned into the pET41b vector, and GST-fusion proteins were produced in *E. coli* BL21(DE3), then purified using glutathione-Sepharose beads (Sigma-Aldrich). Full-length cDNA of *gop-1* was also cloned into the pET21b vector to produce HIS-tagged proteins in *E. coli* BL21(DE3), which were purified using Ni-NTA resin (QIAGEN). pCMV-GOP-1::FLAG was transfected into HEK293T cells to produce GOP-1-FLAG protein, which was purified using anti-FLAG M2 agarose (Sigma-Aldrich).

GST pull-down assay

The wild-type and mutant forms of GST::UNC-108 were immobilized on glutathione-agarose beads, and 3 mM GDP and GTP were loaded onto GST-UNC-108(S20N)– and GST-UNC-108(Q65L)–containing beads, respectively, to lock UNC-108 in the GDP- and GTP-bound conformation. GOP-1-HIS was incubated with immobilized GST-UNC-108(WT), GST-UNC-108(S20N), GST-UNC-108(Q65L), or GST-UNC-108(N119I) for 1 h at 4°C in a buffer containing 50 mM Tris-HCl (pH 7.5), 150 mM NaCl, 1 mM DTT, and 5 mM $MgCl_2$. The resins were washed three times in wash buffer (50 mM Tris-HCl, pH 7.5, 150 mM NaCl, 1 mM DTT, 5 mM $MgCl_2$, and 0.1% CHAPS), and the bound proteins were resolved with SDS-PAGE and detected by immunoblotting using anti-His antibody. The protein level of GST-UNC-108 was revealed by Coomassie blue staining.

Coimmunoprecipitation assay in worms

Adult worms expressing both GFP::GOP-1 and mCherry::UNC-108 or mCherry::UNC-108 alone were lysed with FastPrep-24 (MP Biomedicals) in worm lysis buffer containing 50 mM Tris-HCl, pH 7.5, 150 mM NaCl, 2 mM $MgCl_2$, and protease inhibitor cocktail (EDTA-free; Roche). The homogenized solutions were centrifuged at 1,500 rpm for 10 min at 4°C to remove debris. 500-µl precleared solutions were incubated with 10 µl GBP beads (GFP binding protein; ChromoTek) for 2 h at 4°C. After extensive washing with 50 mM Tris-HCl, pH 7.5, and 150 mM NaCl, the bound proteins were resolved with SDS-PAGE and revealed by Western blotting with antibodies against GFP (Roche) and mCherry (HX1810; Huaxingbio).

Expression and purification of the UNC-108–GDI-1 complex

UNC-108–GDI-1 complex was purified from yeast cells as described before (Machner and Isberg, 2007). In brief, pYES3-FLAG-UNC-108 and pYES2-MYC-HIS-GDI-1 constructs were cotransformed into BCY123 (*MATa*, *Can1*, *ade2*, *trp1*, *Ura3-52*, *his3*, *leu2-3*, *112*, *pep4::his*$^+$, *prb1::leu2*$^+$, *bar1::HisG*$^+$, and *lys2::pGAL1/10-GAL4*$^+$) and selected on SC selective medium lacking tryptophan and uracil (SC-Trp-Ura). A single colony of the transformed yeast was inoculated into SC selective medium containing 2% glucose and grown overnight at 30°C with shaking. Yeast cells were transferred into induction medium (SC selective medium containing 2% galactose and 1% raffinose) at a starting OD_{600} of 1.0 to induce protein expression for 18 h. Cells were then harvested and lysed by FastPrep in a buffer containing 50 mM Tris-HCl, pH 7.5, 150 mM NaCl, and 2 mM $MgCl_2$. The cell lysate was centrifuged and first incubated with Ni-NTA resin for 2 h to separate the FLAG-UNC-108-MYC-HIS-GDI-1 complex from unbound yeast proteins. The bound proteins were eluted with 250 mM imidazole and further incubated with anti-FLAG M2 agarose (Sigma-Aldrich) overnight to separate the FLAG-UNC-108-MYC-HIS-GDI-1 complex from

free MYC-HIS-GDI-1. The bound UNC-108–GDI-1 complex was eluted by addition of 3xFLAG peptides (Sigma-Aldrich).

GTP loading assay

The GTP loading assay was performed as described previously, with modifications (Zhu et al., 2010). 15 pmol UNC-108–GDI-1 complex was incubated with 2 pmol ^{35}S-labeled GTPγS in reaction buffer containing 50 mM Tris-HCl, pH 7.5, 150 mM NaCl, and 2 mM $MgCl_2$ at RT. 15 pmol GOP-1-FLAG was then added to initiate the nucleotide-exchange reaction. Samples were taken at the indicated time points, and the reaction was stopped by adding 500 µl ice-cold wash buffer (50 mM Tris-HCl, 50 mM NaCl, and 2 mM $MgCl_2$). [^{35}S]GTPγS bound to UNC-108 was analyzed by filter binding followed by scintillation counting.

Liposome flotation assay

Recruitment of UNC-108 onto liposomes was analyzed as previously described, with modifications (Wang et al., 2011). In brief, 10 pmol UNC-108–GDI-1 complex was incubated with 1 mM PC liposomes containing 8% PtdIns3P without or with GOP-1 (10 pmol) or GTPγS (100 pmol) as indicated for 2 h at 4°C, followed by a 30-min incubation at RT in a buffer containing 50 mM Tris-HCl, pH 7.5, 150 mM NaCl, and 2 mM $MgCl_2$. The samples were analyzed by sucrose gradient ultracentrifugation. The top layer containing floating PC liposomes was resolved by SDS-PAGE and analyzed by Western blotting.

GDI-1 displacement assay

To examine GDI displacement activity, GST and GST-GOP-1 immobilized on glutathione-agarose beads were incubated with FLAG-UNC-108-MYC-HIS-GDI-1 complex in reaction buffer (50 mM Tris-HCl, pH 7.5, 150 mM NaCl, and 2 mM $MgCl_2$) for 10 min at 25°C followed by centrifugation. The supernatant was collected, and the beads were washed five times. The unbound proteins in the supernatant and proteins bound to beads were subjected to SDS-PAGE and detected by Western blotting. In another experiment, FLAG-UNC-108-MYC-HIS-GDI-1 complex immobilized on FLAG M2 magnetic beads (Sigma-Aldrich) was incubated with GOP-1-HIS for 60 min at 25°C in reaction buffer (50 mM Tris-HCl, pH 7.5, 150 mM NaCl, and 2 mM $MgCl_2$), followed by centrifugation. The supernatant was collected, and the beads were washed five times. The unbound proteins in the supernatant and proteins bound to beads were subjected to SDS-PAGE and detected by Western blotting.

Statistical analysis

The SD was used as *y*-axis error bars for bar charts plotted from the mean value of the data. Data derived from different genetic backgrounds were compared by Student's unpaired *t* test, one-way analysis of variance (ANOVA) followed by Tukey's posttest, or two-way ANOVA followed by Bonferroni posttest, as indicated in the figure legends. Data were considered statistically different at $P < 0.05$.

Table 1. **Primers used for plasmid construction**

Primer	Sequence (5′ to 3′)
PYWW96	GCGGTACCATGTTCCGCAAGCTTGGTTC
PYWW97	GCGGTACCCTAGGATCTTCTTTCCGAAG
PJHY24	CGGCATGCCGACGTACTCCCTATTGCTT
PJHY25	TCCCCCGGGTATCGATTTTGTTCCAGGTT
PPFG656	CGGGTACCATGTTTGGCCGCTCGCGGAGC
PPFG631	CGGGTACCTTACTTGTCATCGTCATCCTTGTAGTCGTCCTCAG CGGTGCCCACAGG
PPFG581	GGAATTCCATATGTTCCGCAAGCTTGGTTCT
PJHY75	GCGGATCCCTAGGATCTTCTTTCCGAAG
PJHY118	GCGGATCCCGGGATCTTCTTTCCGAAGAAC
PPFG626	GCACTAGTATGTTCCGCAAGCTTGGTTCT
PPFG648	CGGGTACCTTACTTGTCATCGTCATCCTTGTAGTCGGATCTTCTTTCCGAAGAAC
PPFG246	GGGGTACCATGGACTACAAGGATGACGATGACAAGTCATATGCCTACCTTTTCAAG
PJHY111	AGCTTTGTTTAAACTTAACAGCATCCAGATCCAC
PJHY94	GGAATTCCATATGATGGATGAGGAATACGATGC
PJHY95	GCGGATCCTTATTCCTGATCATTCAACG
PJHY135	GCGGTACCATGGAACAAAAACTCATCTCAGAAGAGGATCTGCATCATCACCATCACCAC
PPFG81	CCGCTCGAGTTATTCCTGATCATTCAACG
PPFG152	CGCCATGGAGATGTCATATGCCTACCTTTTCAAG
PXCW232	GCGGATCCACAGCATCCAGATCCACCGCCCAATCC
PPFG37	GGGATACTGGAGTAGGAAAAAACTGCTTGCTCCTTCAGTTTAC
PPFG38	GTAAACTGAAGGAGCAAGCAGTTTTTTCCTACTCCAGTATCCC
PPFG39	CAAATTTGGGACACAGCCGGACTAGAATCATTCCGCTCCATC
PPFG40	GATGGAGCGGAATGATTCTAGTCCGGCTGTGTCCCAAATTTG
PPFG51	TATGGTTATTATGTTGATTGGAATTAAGAGTGACCTGGAAGCCCG
PPFG52	CGGGCTTCCAGGTCACTCTTAATTCCAATCAACATAATAACCAT
PXCW259	GCACTAGTATGTCATATGCCTACCTTTTC
PJHY130	GCGGATCCTTAACAGCATCCAGATCCAC
PWZ7	CACTAGCATATGGCCGCCCGAAACGCAGGAACC
PWZ8	GCGGATCCTTATTTACAGCATGAACCCTTTTG
PWZ13	CACTAGCATATGTCGGGAACCAGAAAGAAGGCGC
PWZ14	GCGGATCCTTAACAATTGCATCCCGAATTCTG
PWZ23	CACTAGCATATGACGGCTGCTCCTTACAATTATTC
PWZ24	GCGGATCCCTAGCAGTTGCAGTCCTTCTTCCCAT

Plasmid construction

To generate $P_{ced\text{-}1}$GFP::GOP-1, *gop-1* genomic DNA was amplified by primers PYWW96/PYWW97 and cloned into pPD49.26-$P_{ced\text{-}1}$GFP1 through the KpnI site. To generate $P_{gop\text{-}1}$GFP, the promoter region of *gop-1* (5,020 bp) was amplified using primers PJHY24/PJHY25 and cloned into pPD49.26-GFP through the SphI and BamHI sites. $P_{gop\text{-}1}$GOP-1::GFP was constructed by cloning the *gop-1* genomic sequence into pPD49.26-$P_{gop\text{-}1}$GFP at the XmaI and KpnI sites. To generate $P_{ced\text{-}1}$hCLEC16A-FLAG and $P_{gop\text{-}1}$hCLEC16A-FLAG, human *CLEC16a* was amplified from a human cDNA library using primers PPFG656/PPFG631 and cloned into pPD49.26-$P_{ced\text{-}1}$ and pPD49.26-$P_{gop\text{-}1}$, respectively, through the KpnI site. To generate pGADT7-GOP-1, full-length *gop-1* cDNA was amplified from a *C. elegans* cDNA library using primers PPFG581/PJHY75 and cloned into pGADT7 at the NdeI and BamHI sites. pET21b-GOP-1 was constructed by ligating *gop-1* cDNA amplified using primers PPFG581 and PJHY118 into the pET21b vector at the NdeI and BamHI sites. To generate pET41b-GOP-1, full-length *gop-1* cDNA was amplified using primers PPFG626/PJHY75 and cloned into pET41b at the SpeI and BamHI sites. pCMV-GOP-1-FLAG was constructed by inserting *gop-1-flag* amplified from pGADT7-GOP-1 using primers PYWW96/PPFG648 into pCMY-MYC(-) through the KpnI site. pYES3-FLAG-UNC-108 was constructed by inserting FLAG-UNC-108 amplified by primers PPFG246/PJHY111 into the pYES3 vector at the KpnI and PmeI sites. To generate pET28a-GDI-1, full length cDNA of *gdi-1* was amplified from a *C. elegans* cDNA library using primers pJHY94/PJHY95 and inserted into the pET28a vector at the NdeI and BamHI sites. pYES2-MYC-HIS-GDI-1 was generated by ligating MYC-HIS-GDI-1 amplified from pET28a-GDI-1 by primers PJHY135 and PPFG81 into the pYES2 vector at the KpnI and XhoI sites. To generate pGBKT7-UNC-108, *unc-108* cDNA was amplified from a *C. elegans* cDNA library using primers PPFG152 and PXCW232 and inserted into pGBKT7 at the NcoI–BamHI sites. The S20N, Q65L, and N119I mutations were introduced into pGBKT7-UNC-108 by site-directed mutagenesis (QuikChange; Stratagene) using the primer pairs PPFG37/PPFG38 (S20N), PPFG39/PPFG40 (Q65L), and PPFG51/PPFG52 (N119I). pET41b-UNC-108 (WT/S20N/Q65L/N119I) was constructed by inserting UNC-108 (WT/S20N/Q65L/N119I) amplified from pGBKT7-UNC-108 (WT/S20N/Q65L/N119I) using primers PXCW259/PJHY130 into pET41b at the SpeI–BamHI sites. pGBKT7-RAB-5, pGBKT7-RAB-7, and pGBKT7-RAB-14 were generated by ligating *rab-5*, *rab-7*, and *rab-14* cDNAs amplified from a *C. elegans* cDNA library using primers PWZ7/PWZ8 (RAB-5), PWZ13/PWZ14 (RAB-7), and PWZ23/PWZ24 (RAB-14) into pGBKT7 through the NdeI and BamHI sites (Table 1).

Online supplementary materials

Fig. S1 shows that *gop-1* encodes an evolutionarily conserved protein. Fig. S2 shows that expression of human *CLEC16A* rescues the phagosome, endosome, and locomotion defects of *gop-1* mutants. Fig. S3 shows that *gop-1* is widely expressed. Fig. S4 shows that *gop-1* mutants display defects in endosome and dense core vesicle maturation. Fig. S5 shows that GOP-1 interacts with inactive UNC-108 and disrupts the UNC-108-GDI-1 complex. Video 1 shows that RAB-5 transiently associates with apoptotic cell–containing phagosomes. Video 2 shows that loss of *gop-1* causes prolonged association of RAB-5 with phagosomes. Video 3 shows that PtdIns3P transiently accumulates on phagosomes. Video 4 shows that loss of *gop-1* causes persistent accumulation of PtdIns3P on phagosomes. Video 5 shows that UNC-108 transiently associates with apoptotic cell–containing phagosomes. Video 6 shows that loss of *gop-1* abrogates phagosomal recruitment of UNC-108. Video 7 shows that UNC-108 transiently associates with endosomes in coelomocytes. Video 8 shows that loss of *gop-1* abolishes recruitment of UNC-108 to endosomes. Table S1 shows that loss of *tbc-2* enhances the somatic cell corpse phenotype of *gop-1* and *unc-108* mutants. Table S2 shows that loss of *sand-1* enhances the germ cell corpse phenotype of *gop-1* and *unc-108* mutants.

Acknowledgments

We thank Drs. K. Ravichandran, M.O. Hengartner, B. Grant, H. Fares, K.G. Miller, J.M. Kaplan, and Z. Bao for strains and Dr. Isabel Hanson for editing services.

Some strains were provided by the Caenorhabditis Genetics Center, which is funded by the National Institutes of Health Office of Research Infrastructure Programs (P40OD010440). This work was supported by the National Science Foundation of China (31325015), the National Basic Research Program of China (2013CB910100 and 2014CB849702), the Strategic Priority Research Program of the Chinese Academy of Sciences (XDB19000000), Chinese Ministry of Science and Technology (2016YFA0500203), and an International Early Career Scientist grant from the Howard Hughes Medical Institute to X. Wang.

The authors declare no competing financial interests.

Author Contributions: J. Yin and Y. Huang performed and designed experiments along with X. Wang and P. Guo, and S. Hu performed some of the genetic and cell biological experiments. S. Yoshina, N. Xuan, Q. Gan, S. Mitani, and C. Yang contributed to the generation of strains. X. Wang wrote the paper with input from J. Yin, C. Yang, and S. Mitani.

Submitted: 1 October 2016
Revised: 10 February 2017
Accepted: 3 March 2017

References

Barr, F.A. 2013. Review series: Rab GTPases and membrane identity: Causal or inconsequential? *J. Cell Biol.* 202:191–199. http://dx.doi.org/10.1083/jcb.201306010

Barr, F., and D.G. Lambright. 2010. Rab GEFs and GAPs. *Curr. Opin. Cell Biol.* 22:461–470. http://dx.doi.org/10.1016/j.ceb.2010.04.007

Cabrera, M., and C. Ungermann. 2013. Guanine nucleotide exchange factors (GEFs) have a critical but not exclusive role in organelle localization of Rab GTPases. *J. Biol. Chem.* 288:28704–28712. http://dx.doi.org/10.1074/jbc.M113.488213

Cheng, S., K. Wang, W. Zou, R. Miao, Y. Huang, H. Wang, and X. Wang. 2015. PtdIns(4,5)P_2 and PtdIns3P coordinate to regulate phagosomal sealing for apoptotic cell clearance. *J. Cell Biol.* 210:485–502. http://dx.doi.org/10.1083/jcb.201501038

Cheng, S., K. Liu, C. Yang, and X. Wang. 2017. Dissecting phagocytic removal of apoptotic cells in *Caenorhabditis elegans*. *Methods Mol. Biol.* 1519:265–284. http://dx.doi.org/10.1007/978-1-4939-6581-6_18

Cherfils, J., and M. Zeghouf. 2013. Regulation of small GTPases by GEFs, GAPs, and GDIs. *Physiol. Rev.* 93:269–309. http://dx.doi.org/10.1152/physrev.00003.2012

Chun, D.K., J.M. McEwen, M. Burbea, and J.M. Kaplan. 2008. UNC-108/Rab2 regulates postendocytic trafficking in *Caenorhabditis elegans*. *Mol. Biol. Cell.* 19:2682–2695. http://dx.doi.org/10.1091/mbc.E07-11-1120

Delprato, A., and D.G. Lambright. 2007. Structural basis for Rab GTPase activation by VPS9 domain exchange factors. *Nat. Struct. Mol. Biol.* 14:406–412. http://dx.doi.org/10.1038/nsmb1232

Dirac-Svejstrup, A.B., T. Sumizawa, and S.R. Pfeffer. 1997. Identification of a GDI displacement factor that releases endosomal Rab GTPases from Rab-GDI. *EMBO J.* 16:465–472. http://dx.doi.org/10.1093/emboj/16.3.465

Edwards, S.L., N.K. Charlie, J.E. Richmond, J. Hegermann, S. Eimer, and K.G. Miller. 2009. Impaired dense core vesicle maturation in *Caenorhabditis elegans* mutants lacking Rab2. *J. Cell Biol.* 186:881–895. http://dx.doi.org/10.1083/jcb.200902095

Farnsworth, C.C., M.C. Seabra, L.H. Ericsson, M.H. Gelb, and J.A. Glomset. 1994. Rab geranylgeranyl transferase catalyzes the geranylgeranylation of adjacent cysteines in the small GTPases Rab1A, Rab3A, and Rab5A. *Proc. Natl. Acad. Sci. USA.* 91:11963–11967. http://dx.doi.org/10.1073/pnas.91.25.11963

Flannagan, R.S., V. Jaumouillé, and S. Grinstein. 2012. The cell biology of phagocytosis. *Annu. Rev. Pathol.* 7:61–98. http://dx.doi.org/10.1146/annurev-pathol-011811-132445

Gengyo-Ando, K., and S. Mitani. 2000. Characterization of mutations induced by ethyl methanesulfonate, UV, and trimethylpsoralen in the nematode *Caenorhabditis elegans*. *Biochem. Biophys. Res. Commun.* 269:64–69. http://dx.doi.org/10.1006/bbrc.2000.2260

Gumienny, T.L., E. Lambie, E. Hartwieg, H.R. Horvitz, and M.O. Hengartner. 1999. Genetic control of programmed cell death in the *Caenorhabditis elegans* hermaphrodite germline. *Development.* 126:1011–1022.

Guo, P., T. Hu, J. Zhang, S. Jiang, and X. Wang. 2010. Sequential action of *Caenorhabditis elegans* Rab GTPases regulates phagolysosome formation during apoptotic cell degradation. *Proc. Natl. Acad. Sci. USA.* 107:18016–18021. http://dx.doi.org/10.1073/pnas.1008946107

Gutierrez, M.G. 2013. Functional role(s) of phagosomal Rab GTPases. *Small GTPases.* 4:148–158. http://dx.doi.org/10.4161/sgtp.25604

Hakonarson, H., S.F. Grant, J.P. Bradfield, L. Marchand, C.E. Kim, J.T. Glessner, R. Grabs, T. Casalunovo, S.P. Taback, E.C. Frackelton, et al. 2007. A genome-wide association study identifies KIAA0350 as a type 1 diabetes gene. *Nature.* 448:591–594. http://dx.doi.org/10.1038/nature06010

Hoppenbrouwers, I.A., Y.S. Aulchenko, A.C. Janssens, S.V. Ramagopalan, L. Broer, M. Kayser, G.C. Ebers, B.A. Oostra, C.M. van Duijn, and R.Q. Hintzen. 2009. Replication of CD58 and CLEC16A as genome-wide significant risk genes for multiple sclerosis. *J. Hum. Genet.* 54:676–680. http://dx.doi.org/10.1038/jhg.2009.96

Horiuchi, H., R. Lippé, H.M. McBride, M. Rubino, P. Woodman, H. Stenmark, V. Rybin, M. Wilm, K. Ashman, M. Mann, and M. Zerial. 1997. A novel Rab5 GDP/GTP exchange factor complexed to Rabaptin-5 links nucleotide exchange to effector recruitment and function. *Cell.* 90:1149–1159. http://dx.doi.org/10.1016/S0092-8674(00)80380-3

Ingmundson, A., A. Delprato, D.G. Lambright, and C.R. Roy. 2007. *Legionella pneumophila* proteins that regulate Rab1 membrane cycling. *Nature.* 450:365–369. http://dx.doi.org/10.1038/nature06336

Kim, S., Y.P. Wairkar, R.W. Daniels, and A. DiAntonio. 2010. The novel endosomal membrane protein Ema interacts with the class C Vps-HOPS complex to promote endosomal maturation. *J. Cell Biol.* 188:717–734. http://dx.doi.org/10.1083/jcb.200911126

Kim, S., S.A. Naylor, and A. DiAntonio. 2012. *Drosophila* Golgi membrane protein Ema promotes autophagosomal growth and function. *Proc. Natl. Acad. Sci. USA.* 109:E1072–E1081. http://dx.doi.org/10.1073/pnas.1120320109

Kinchen, J.M., and K.S. Ravichandran. 2010. Identification of two evolutionarily conserved genes regulating processing of engulfed apoptotic cells. *Nature.* 464:778–782. http://dx.doi.org/10.1038/nature08853

Kinchen, J.M., K. Doukoumetzidis, J. Almendinger, L. Stergiou, A. Tosello-Trampont, C.D. Sifri, M.O. Hengartner, and K.S. Ravichandran. 2008. A pathway for phagosome maturation during engulfment of apoptotic cells. *Nat. Cell Biol.* 10:556–566. http://dx.doi.org/10.1038/ncb1718

Kucharczyk, R., A.M. Kierzek, P.P. Slonimski, and J. Rytka. 2001. The Ccz1 protein interacts with Ypt7 GTPase during fusion of multiple transport intermediates with the vacuole in *S. cerevisiae*. *J. Cell Sci.* 114:3137–3145.

Li, W., W. Zou, D. Zhao, J. Yan, Z. Zhu, J. Lu, and X. Wang. 2009. C. elegans Rab GTPase activating protein TBC-2 promotes cell corpse degradation by regulating the small GTPase RAB-5. *Development.* 136:2445–2455. http://dx.doi.org/10.1242/dev.035949

Lu, Q., Y. Zhang, T. Hu, P. Guo, W. Li, and X. Wang. 2008. *C. elegans* Rab GTPase 2 is required for the degradation of apoptotic cells. *Development.* 135:1069–1080. http://dx.doi.org/10.1242/dev.016063

Machner, M.P., and R.R. Isberg. 2007. A bifunctional bacterial protein links GDI displacement to Rab1 activation. *Science.* 318:974–977. http://dx.doi.org/10.1126/science.1149121

Mangahas, P.M., X. Yu, K.G. Miller, and Z. Zhou. 2008. The small GTPase Rab2 functions in the removal of apoptotic cells in *Caenorhabditis elegans*. *J. Cell Biol.* 180:357–373. http://dx.doi.org/10.1083/jcb.200708130

Márquez, A., J. Varadé, G. Robledo, A. Martínez, J.L. Mendoza, C. Taxonera, M. Fernández-Arquero, M. Díaz-Rubio, M. Gómez-García, M.A. López-Nevot, et al. 2009. Specific association of a CLEC16A/KIAA0350 polymorphism with NOD2/CARD15(-) Crohn's disease patients. *Eur. J. Hum. Genet.* 17:1304–1308. http://dx.doi.org/10.1038/ejhg.2009.50

Musha, T., M. Kawata, and Y. Takai. 1992. The geranylgeranyl moiety but not the methyl moiety of the smg-25A/rab3A protein is essential for the interactions with membrane and its inhibitory GDP/GTP exchange protein. *J. Biol. Chem.* 267:9821–9825.

Pereira-Leal, J.B., and M.C. Seabra. 2000. The mammalian Rab family of small GTPases: Definition of family and subfamily sequence motifs suggests a mechanism for functional specificity in the Ras superfamily. *J. Mol. Biol.* 301:1077–1087. http://dx.doi.org/10.1006/jmbi.2000.4010

Pfeffer, S., and D. Aivazian. 2004. Targeting Rab GTPases to distinct membrane compartments. *Nat. Rev. Mol. Cell Biol.* 5:886–896. http://dx.doi.org/10.1038/nrm1500

Pinto, S.M., and M.O. Hengartner. 2012. Cleaning up the mess: Cell corpse clearance in *Caenorhabditis elegans*. *Curr. Opin. Cell Biol.* 24:881–888. http://dx.doi.org/10.1016/j.ceb.2012.11.002

Savill, J., and V. Fadok. 2000. Corpse clearance defines the meaning of cell death. *Nature.* 407:784–788. http://dx.doi.org/10.1038/35037722

Savill, J., I. Dransfield, C. Gregory, and C. Haslett. 2002. A blast from the past: Clearance of apoptotic cells regulates immune responses. *Nat. Rev. Immunol.* 2:965–975. http://dx.doi.org/10.1038/nri957

Schoebel, S., L.K. Oesterlin, W. Blankenfeldt, R.S. Goody, and A. Itzen. 2009. RabGDI displacement by DrrA from *Legionella* is a consequence of its guanine nucleotide exchange activity. *Mol. Cell.* 36:1060–1072. http://dx.doi.org/10.1016/j.molcel.2009.11.014

Seabra, M.C., and C. Wasmeier. 2004. Controlling the location and activation of Rab GTPases. *Curr. Opin. Cell Biol.* 16:451–457. http://dx.doi.org/10.1016/j.ceb.2004.06.014

Sivars, U., D. Aivazian, and S.R. Pfeffer. 2003. Yip3 catalyses the dissociation of endosomal Rab-GDI complexes. *Nature.* 425:856–859. http://dx.doi.org/10.1038/nature02057

Skinningsrud, B., E.S. Husebye, S.H. Pearce, D.O. McDonald, K. Brandal, A.B. Wolff, K. Løvås, T. Egeland, and D.E. Undlien. 2008. Polymorphisms in CLEC16A and CIITA at 16p13 are associated with primary adrenal insufficiency. *J. Clin. Endocrinol. Metab.* 93:3310–3317. http://dx.doi.org/10.1210/jc.2008-0821

Soleimanpour, S.A., A. Gupta, M. Bakay, A.M. Ferrari, D.N. Groff, J. Fadista, L.A. Spruce, J.A. Kushner, L. Groop, S.H. Seeholzer, et al. 2014. The diabetes susceptibility gene Clec16a regulates mitophagy. *Cell.* 157:1577–1590. http://dx.doi.org/10.1016/j.cell.2014.05.016

Suh, H.Y., D.W. Lee, K.H. Lee, B. Ku, S.J. Choi, J.S. Woo, Y.G. Kim, and B.H. Oh. 2010. Structural insights into the dual nucleotide exchange and GDI displacement activity of SidM/DrrA. *EMBO J.* 29:496–504. http://dx.doi.org/10.1038/emboj.2009.347

Sumakovic, M., J. Hegermann, L. Luo, S.J. Husson, K. Schwarze, C. Olendrowitz, L. Schoofs, J. Richmond, and S. Eimer. 2009. UNC-108/RAB-2 and its effector RIC-19 are involved in dense core vesicle maturation in *Caenorhabditis elegans*. *J. Cell Biol.* 186:897–914. http://dx.doi.org/10.1083/jcb.200902096

van Luijn, M.M., K.L. Kreft, M.L. Jongsma, S.W. Mes, A.F. Wierenga-Wolf, M. van Meurs, M.J. Melief, R. der Kant, L. Janssen, H. Janssen, et al. 2015. Multiple sclerosis-associated CLEC16A controls HLA class II expression via late endosome biogenesis. *Brain.* 138:1531–1547. http://dx.doi.org/10.1093/brain/awv080

Wang, X., and C. Yang. 2016. Programmed cell death and clearance of cell corpses in *Caenorhabditis elegans*. *Cell. Mol. Life Sci.* 73:2221–2236. http://dx.doi.org/10.1007/s00018-016-2196-z

Wang, T., Y. Liu, X.H. Xu, C.Y. Deng, K.Y. Wu, J. Zhu, X.Q. Fu, M. He, and Z.G. Luo. 2011. Lgl1 activation of rab10 promotes axonal membrane trafficking underlying neuronal polarization. *Dev. Cell.* 21:431–444. http://dx.doi.org/10.1016/j.devcel.2011.07.007

Wang, X., C. Yang, J. Chai, Y. Shi, and D. Xue. 2002. Mechanisms of AIF-mediated apoptotic DNA degradation in *Caenorhabditis elegans*. *Science.* 298:1587–1592. http://dx.doi.org/10.1126/science.1076194

Wang, X., J. Wang, K. Gengyo-Ando, L. Gu, C.L. Sun, C. Yang, Y. Shi, T. Kobayashi, Y. Shi, S. Mitani, et al. 2007. C. elegans mitochondrial factor WAH-1 promotes phosphatidylserine externalization in apoptotic cells through phospholipid scramblase SCRM-1. *Nat. Cell Biol.* 9:541–549. http://dx.doi.org/10.1038/ncb1574

Xiao, H., D. Chen, Z. Fang, J. Xu, X. Sun, S. Song, J. Liu, and C. Yang. 2009. Lysosome biogenesis mediated by vps-18 affects apoptotic cell degradation in *Caenorhabditis elegans*. *Mol. Biol. Cell.* 20:21–32. http://dx.doi.org/10.1091/mbc.E08-04-0441

Yu, X., N. Lu, and Z. Zhou. 2008. Phagocytic receptor CED-1 initiates a signaling pathway for degrading engulfed apoptotic cells. *PLoS Biol.* 6:e61. http://dx.doi.org/10.1371/journal.pbio.0060061

Zhang, Y., B. Grant, and D. Hirsh. 2001. RME-8, a conserved J-domain protein, is required for endocytosis in *Caenorhabditis elegans*. *Mol. Biol. Cell.* 12:2011–2021. http://dx.doi.org/10.1091/mbc.12.7.2011

Zhu, Y., L. Hu, Y. Zhou, Q. Yao, L. Liu, and F. Shao. 2010. Structural mechanism of host Rab1 activation by the bifunctional *Legionella* type IV effector SidM/DrrA. *Proc. Natl. Acad. Sci. USA.* 107:4699–4704. http://dx.doi.org/10.1073/pnas.0914231107